Optimal design of lithium ion battery thermal management systems based on phase change material at high current and high environmental temperature

Girolama Airò Farulla , Valeria Palomba [*], Davide Aloisio , Giovanni Brunaccini , Marco Ferraro , Andrea Frazzica , Francesco Sergi

CNR – ITAE - Istituto di Tecnologie Avanzate per l'Energia "Nicola Giordano", Salita S. Lucia sopra Contesse 5, Messina 98126, Italy

ARTICLE INFO

ABSTRACT

The market of electric storage systems is widely dominated by Lithium ion batteries, whose peculiarity is the need for a thermal management system, whose proper design is complicated by the interaction. among different design and operating parameters. A specific methodology for carrying out the task is still lacking. In this context, the present paper proposes a systematic framework for the design of passive and hybrid thermal management systems (TMSs) of Li-ion batteries. Thermal tests were carried out on Lithium-Titanate-Oxide cells under realistic operating conditions in a controlled environment to characterize the electrical and thermal behaviour. A thermofluid dynamics model of the battery was implemented in COMSOL Multiphysics. The experimentally validated model was used to evaluate the influence of different design and operating parameters (ambient temperature, charge/discharge current, phase change material thickness and melting temperature) using the Taguchi method (orthogonal arrays), and discussing inter-related effects of the studied parameters via interaction plots. Air temperature (45 °C) and/or discharge current (69–92 A) were identified as critical operating conditions beyond which thermal runaway issues occur. Starting from the optimal design conditions for a passive TMS, the same methodology was used to assess a hybrid PCM-liquid cooling system as an alternative configuration. The results indicate that, compared to the baseline case of natural cooling, the optimal designs of standalone PCM and hybrid cooling system led to a reduction in maximum cell temperature of 11 and 22 °C, respectively, showing the high potential of these TMSs.

Introduction

Electrification of the energy and mobility sector has determined a strong boost on the development and commercialization of electric storage systems [1]. The vast majority of the market is dominated by Li-ion batteries, which strongly suffer the operation under extreme temperatures, both high and low ones (i.e. T > 60 °C and T < 5 °C) [2–4]. When the thermal stress on the battery exceeds the safety limits there is a higher risk for the thermal runaway of the system [5–7]. The modifications/additions to the chemistry of the battery (i.e. through the modifications of the electrodes) and the use of an external management system are examples of solutions proposed to reduce the thermal stress on the batteries [8]. A critical point is the dependence of the safety conditions from the external ambient temperature, for which data and proper designs are still lacking.

The thermal dissipation of the cell is due to irreversible and reversible heat [9]. The irreversible heat is energy generated from resistive dissipation and polarization phenomena while that reversible is due to entropy changes caused by the electrochemical reactions. The thermal safety is a crucial prerequisite for the practical applications of the Li-ion batteries [10,11]. This task can be achieved through the use of a proper battery thermal management system (TMS).

The design of a thermal management system cannot preclude from the knowledge and modelling of the thermal behaviour of the cell. In recent years, different ways have been proposed for such a purpose, including coupled electrochemical-thermal models [12–14], Computational Fluid Dynamic (CFD) based models [15,16] and lumped thermal models [17,18]. Lumped models are computationally less expensive but are less accurate in the prediction of the behavior of the cell. CFD modelling is mainly used to achieve detailed results for the temperature distribution and to provide optimal solutions during hazardous

Nomenclature

Cap	Capacity [Ah]
cp	Specific heat [kJ/(kg K)]
F	Factor
g	Gravity constant [m/s^2]
H	Heat capacity of PCM [J/kg]
h	Convective coefficient [W/(m^{2}K)]
i	Current [A]
k	Thermal conductivity [W/(m K)]
L	Level
Q	Thermal power [W]
q$''$	Heat flux [W/m^2]
q$'''$	Volumetric heat source [W/m^3]
n	normal
p	Pressure, Pa
S/N	Signal to noise ratio [dB]
s	Thickness [m]
T	Temperature [K]
t	time [s]
u	Velocity [m/s]
V	Voltage [V]
Vol	Volume [m^3]

Greek letters

α	Liquid fraction
ß	Phase change enthalpy [J/kg]
η	Cooling efficiency
ρ	Density [kg/m^3]
μ	Dynamic viscosity [Pa s]

Subscripts

amb	Ambient
atm	Atmospheric
av	Average
b	Battery
c	Cell
con	Convective
cr	Crystallization
d	Discharge
f	Fluid
hyb	Hybrid
In	Inlet
irr	Irreversible
max	Maximum
mel	Melting
min	Minimum
n	Nominal
pc	Phase change material
rev	Reversible
s	Surface
w	Water

Abbreviations

ANN	Artificial neural networks
CFD	Computational Fluid Dynamics
DoD	Depth of discharge
HPPC	Hybrid Power Pulse Characterization
IR	Infrared
LB	Larger the better
LTO	Lithium-titanate-oxide
MBE	Mean bias error
NB	Nominal the better
OCV	Open Circuit Voltage
PCM	Phase Change Material
PLC	Programmable logic controller
Re	Reynolds number
RMSE	Root mean square error
SB	Smaller the better
SoC	State of Charge
TMS	Thermal Management System

scenarios of the Li-ion batteries [19]. The application of artificial neural networks (ANN) in the Li-ion batteries modelling is still relatively new [20–24].

The parameters needed for the thermal modelling of the batteries are usually identified experimentally, mainly calorimetric methods and potentiometric methods [25,26]. These methods require a long test time and expensive equipment. Recently new faster methods have been proposed for the estimation of the thermal parameters. For instance, Wang et al. [27] proposed a novel model based on temperature rise responses of galvanostatic discharge tests with different discharge currents. Parameters are analytically calculated based on combined electric and thermal gradient tests.

Experimental methods are usually carried out or in a climatic chamber under conditions which are not representative of operating conditions [27] or in ambient air under variable operating conditions [28]. Accordingly, reliable data for test experiments under controlled temperature conditions and fast charge/discharge operation are lacking.

The thermal management systems discussed in the literature can be mainly divided in three categories [29,30]:

- Active systems, using liquid heat transfer medium, heat pipes and forced air for heating/cooling;
- Passive management systems, consisting mainly of Phase Change Materials (PCM)-based heating/cooling;
- Hybrid systems, conceived as a combination of the previous cases.

PCM-based systems are preferred to active ones so the high level of heat absorption potential of the PCM provides more temperature distribution [24]. The main advantage of the passive thermal management, as reported in Teichert et al. [31], is the cost-effectiveness compared to the other designs. For instance, Teichert et al. [31] performed a comparative analysis between an active cooling system with fans and a passive one for climates with high temperatures and humidity. They showed how the operational costs of the auxiliaries needed to drive the active cooling system, or the investment costs if systems like heat pipes are used, make the passive system selection as the optimal choice from operational easiness and cost perspectives.

Numerical analyses available in the literature related to PCM-based TMSs mainly focus on the optimization of the material [32,33], in terms of the choice of the most suitable PCM [34] and, more frequently, on the enhancement of the heat transfer through the use of conductive nanoparticles [35], metallic open structures, e.g. metal foams [36–38] or metallic fins [39,40]. The main drawback of most of such methods is the high-cost of the fillers or matrices used, especially in case of nanoparticles or the difficulties in the realization of the finned structures proposed. For instance, Weng et al. [41], demonstrated that the use of branched fins is a suitable method for reducing the temperature of cells working at high ambient temperatures (40 °C) by up to 5 K. However, the realization of such structures is complex and can significantly affect the cost-effectiveness of the solutions. Zhang et al. [42,43] proposed as alternative method the use of flexible PCMs consisting of a composite of boron nitride and rubber. These systems, still far from possible market

deployment, have both a thermal management and mechanical stress reduction purposes and are able to keep the temperature of the battery within acceptable safety range.

In order to properly design passive TMSs, parametric analyses on the main design parameters are often presented in the literature. For instance, Lamrani et al. [34], performed a sensitivity analysis in ANSYS to investigate the effect of melting temperature and thickness of the PCM on the battery temperature during both charge and discharge cycles. PCM with a transition temperature 32 °C was identified as a suitable solution allowing a reduction of the maximum battery temperature up to 3°CA reduction in the maximum temperature up 1.6 °C was found increasing the PCM conductance. Verma et al. [44] carried out numerical simulations in Ansys to perform a sensitivity analysis on ambient conditions, thickness of the PCM and discharge rate. The effect on the maximum temperature was investigated. PCM layer of 3 mm thickness was identified as the optimum for both moderate and desert climates conditions. Zhao et al. [45] proposed the design of a PCM-filled mandrel for the thermal management of Li-ion batteries. Investigated aspects include PCM selection, PCM core size and distribution under the final goal of finding the most compact solution that allows safe operation of the battery. To this aim, different combinations of the parameters are simulated in COMSOL Multiphysics software through several runs. For each parameter, a battery performance index was calculated and the parameters for the space-saving design are discussed.

As shown by the above literature, one of the critical points not usually addressed is the selection of the PCM. Indeed, all the works mentioned are either using the data for paraffinic materials or paraffine waxes with thermal conductivity enhancers (e.g. metal foams, metal particles.). However, paraffines are flammable materials and their application in combination with batteries poses some security questions that cannot be neglected in a commercial perspective. Furthermore, it is worth noticing that the evaluations discussed above are mainly based on parametric analyses carried out on numerical model by simply running the model with the different input parameters and the results are then discussed, but there is no framework for design or specific methodology applied for the systematic evaluation of the most relevant parameters and their mutual effect.

Regarding hybrid thermal management systems, these are able to take advantage of both active and passive cooling TMSs to achieve a better battery temperature uniformity and a higher energy efficiency [46]. Recent advancements are extensively described in [47,48]. The most common methods employed include the combination or air cooling with PCMs [49], the combination of liquid cooling with PCMs or the use of heat pipes [50,51] and thermoelectric coolers in combination with PCMs [52]. The combination of liquid cooling and PCMs is however the most studied one [48].

In general, the investigations available in the literature related to hybrid TMSs are mainly focus on the design of the cooling plate. For instance, Yang et al. [46] analysed nine different cooling plates(one without PCM), differing for the number of channels for water passages. The average surface temperature and total power consumption of battery of each design are analysed and compared. The system with the higher number of branches allowed 50% improvement of cooling performance. Faizan et al. [53] analysed different designs of cold plates showing that as long as Reynolds number for different designs keep in the same range, similar performance in terms of temperature uniformity can be reached. Zhao et al. [54] carried out a similar analysis on the effect of Reynolds. The main finding is that the optimal Reynolds number depends on the charge/discharge rate of the battery. Zhuang et al. [55] presented a hybrid system with PCM and cooling plates arranged in honeycomb manner. An analysis is carried out on the number of channels for optimal cooling by dedicated simulations on each configuration. The result indicated that high channel number has a low effect on the temperature uniformity of the battery. Operational parameters for the liquid cooling portion of the hybrid systems are important as well. Wang et al. [56] performed a parametric study, for

the same system coupling PCMs and microchannel cold plate in parallel and cross flow configurations. It was found that there exists an optimum flow rate, which is depending on the melting temperature of the PCM used for the hybrid cooling system. Moreover, cross flow configuration allows much better cooling performance and temperature uniformity as well as an improvement of the utilization rate of PCM. The same authors improved the hybrid system considering the addition of metallic fins on the external side of the battery [57]. The results indicated a reduction of the temperature difference in the battery pack by 69%. Cell arrangement variation (triangular and rectangular) is proposed as an alternative thermal management strategy in the work of Alharbi et al. [58]. It was found that optimal cooling is achieved by combining triangular arrangement and identifying the optimal Reynolds for the cooling plate. Behi et al. [59] analysed experimentally the fast charging of lithium-titanate-oxide (LTO) batteries. Three hybrid systems are compared: natural convection, PCM buffer only and PCM + liquid cooling. The effect of PCM only is in the order of 15% average temperature reduction, while with hybrid cooling up to 26% reduction can be achieved.

Similar to the case of passive battery management systems, the evaluation on the hybrid ones is mostly carried out by combined numerical and experimental activities or by means of CFD modelling. The main limitations are the evaluation of high charge/discharge rates and multiple cycling only in some of the works and, in the majority of cases, only numerically, without any experimental support to the conclusions. Critical evaluations are mostly based on the results of the numerical analysis rather than by proposing a proper design framework for the systems.

Gap identification and motivation for the research

From the above-reported literature analysis, it clearly emerges that efforts on the optimal design of TMSs have been put in the recent years. However, the aspects missing in most of the analysis are:

- The identification of a systematic method for the design of the system, that allows the selection of the optimal parameters for the foreseen application without having to perform several simulations. Moreover, especially for the hybrid systems discussed above, it is clear from the current investigations that there is a strong correlation between the various design and operating parameters (e.g. Reynolds number and PCM melting temperature). Such an aspect requires a dedicated analysis;
- The evaluation of the operation under high-current applications, conditions under which thermal degradation can more easily affect the proper operation and capacity of the battery [34];
- The effect of multiple cycles in the heating of the battery;
- The reasoned selection and use of PCMs that poses no safety threats due to flammability.

Indeed, as to the best authors' knowledge, there are no literature reviews or papers that propose a specific methodology for the design of thermal management systems. Indeed, considering the investigations available in the literature, all the guidelines for the design of the TMSs are based on simulations carried out on the specific case under evaluation or through parametric analyses of CFD models, which are time and resource expensive. Machine learning techniques have also been proposed, but again specifically focused on the TMS designed by the authors of each research [60,61].

The present paper seeks to address all the challenges identified. Accordingly, we propose to cover the gap regarding the formulation of a systematic framework for the design of TMSs by combining numerical and experimental methods. To further improve the reproducibility of the analysis and the usefulness of results, Taguchi method was used for the systematic evaluation of different operating and design factors and their inter-related influence was discussed, which represents a novelty in the literature [62].

Moreover, the experimental activity carried out is focused on Lithium-Titanate-Oxide cells tested under high-temperature (up to 45 °C) and high-current conditions (up to 4C) [63]. Indeed, literature data under these conditions are not available under controlled ambient boundaries.

The results from the experimental tests in a climatic chamber under variable operating currents and temperatures were used for the calibration of a thermal model of the battery. A passive TMS system was then designed according to the proposed methodology. Specific focus was put on the selection of the PCM to be used, selecting and experimentally testing some low-flammability bio-based PCMs. Finally, starting from the optimal design conditions for a passive TMS, the improvement of the TMS by combining the PCM with water cooling in a hybrid system is discussed, again using the Taguchi method for an optimization of the main design parameters, to show the potentiality of the methodology followed also for this category of TMS.

Methodology

As previously remarked, several works in the literature deal with the design of the thermal management solutions for Li-ion batteries in different scales and applications. What is evidently missing, though, is the clear identification of a methodology that, with reasonable time and computational efforts, can allow an efficient design. Accordingly, in the present work a new method is proposed which consists of the following steps:

1. Identification of different design and operating parameters affecting the operation for a passive TMS;
2. Development and validation of a thermal model for the cell;
3. Use of Taguchi approach for the identification of the minimum representative set of conditions to be simulated to evaluate the effect of the parameters selected;
4. Derivation of the interaction plot and calculation of S/N ratios for the analysis of the most influential parameters on the system operation. Such a step represents the first outcome of the proposed approach and can be used for the design of the most effective passive TMS for the investigated conditions;
5. Taking into account the results of the previous step (i.e. considering the worst operating conditions and the most efficient design parameters), a subsequent evaluation of a hybrid TMS with PCM and liquid cooling was carried out using the same methodology. Taguchi orthogonal array method was used for the selection of the representative conditions and the S/N ratios for the various cases were calculated;
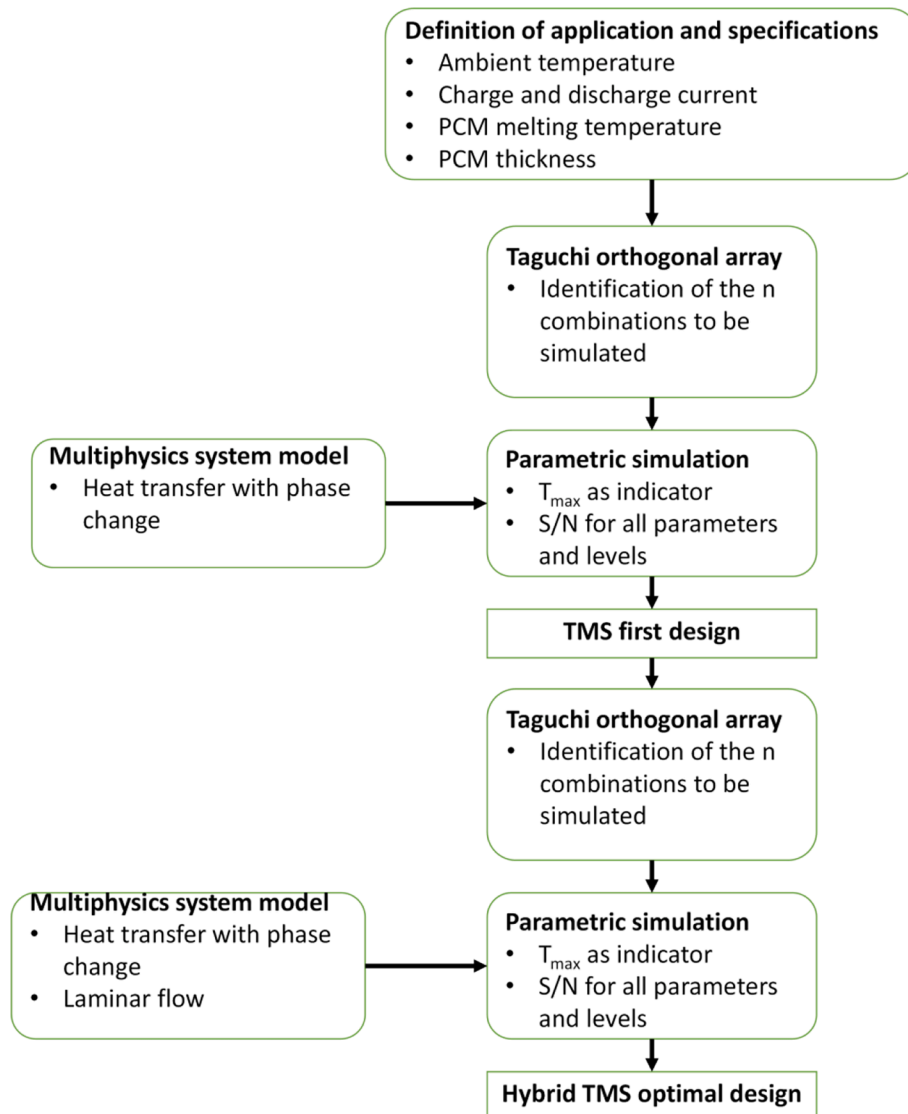

Fig. 1. Methodology.

6. Outcome of the activity was a validated TMS for applications that are uncommon in the literature that can improve the capacity and safety in battery operation upon repeated cycles at high current.

The methodology is reported in Fig. 1.

Experimental

The experimental activity carried out consisted in the evaluation of the thermal behaviour of a Lithium-Titanate Oxide cell under different ambient temperatures and charge/discharge conditions High-power applications, such as electric mobility and peak-shaving are considered in this following investigation, with the aim to improve the overall efficiency and possible user scenarios as compared to a standard system.

Materials

The main features of the tested cell are reported in Table 1.

The passive thermal management system consists of a layer of PCM around the lateral surfaces of the cell and enclosed within a metal thin shell. One of the investigated parameters for the optimization of the system is the selected PCM. Bio-based PCMs from Croda® were considered for the application. The main features of the PCMs selected are reported in Table 2.

In addition, the case of a PCM with melting temperature of 40 °C was considered for sensitivity purposes. Given the fact that the range of variation of the thermal properties of the investigated PCM is within 10% when passing from CrodaTherm™37 to CrodaTherm™47, a fictious material with melting temperature of 40 °C and the same thermal properties of CrodaTherm™37 was considered in the analysis.

It is worth noticing that the main difference between the PCMs evaluated in this work and the ones usually employed in the studies available in the literature is the fact that they are bio-based ones. Only a limited amount of bio-based PCMs is available commercially, but the peculiarity of those considered in the present analysis is the low flammability, which is a critical issue in the application within battery TMS. Therefore, despite several studies discuss the optimal melting point of the PCM for the application, it was considered worthy of investigation to make a parametric study on this aspect as well.

Table 1
Features of the tested cell.

Nominal Capacity [Ah]	23
Nominal Voltage [V]	2.3
Dimensions [mm]	$116 \times 22 \times 106$
Anode material	LTO ($Li_4Ti_5O_{12}$)
Material cathode	NCM ($LiNi_{0.5}Co_{0.2}Mn_{0.3}O_2$)
Material electrolyte	Carbonate based

Table 2
Features of the pcms selected for the evaluation.

	CrodaTherm™32	CrodaTherm™37	CrodaTherm™47
Melting temperature [°C]	32.0	36.8	47.0
Crystallization temperature [°C]	29.5	35.0	45.0
Latent heat capacity [kJ/kg]	223	216	210
Density [kg/m³]	916 (solid)836 (liquid)	957 (solid)819 (liquid)	940 (solid) 829 (liquid
Specific heat capacity [kJ/(kg/K)]	2.3 (solid)1.4 (liquid)	2.3 (solid)1.4 (liquid)	1.9 (solid)2.0 (liquid)
Thermal conductivity [W/(m K)]	0.22 (solid)0.16 (liquid)	0.24 (solid)0.17 (liquid)	0.25 (solid)0.16 (liquid)

Table 3
Features of the Angelantoni climatic chamber used for environmental conditioning during testing.

Electric features	
Phases	3P + N + PE
Nominal Voltage [V]	400
Voltage Tolerance [%]	10
Frequency [%]	50
Maximum Current [A]	21
Degree of protection	IP 22
General information	
Volume [l]	559
Internal sizes [L × W × H]	850 × 740 × 890
External sizes [L × W × H]	1168 × 1797 × 2021
Power installed [kW]	11,4
Supply Voltage	400 ± 10%/50 Hz/3ph + N + T
Weight [kg]	930
Climatic features	
Temperature range [°C]	−40/+180
Humidity range [%]	10/98 (+5/+95 °C)
Dew point [°C]	+2/+94
Max Temperature variation	4,5 °C/min (-40/+180 °C) 4 °C/min (+180/-40 °C)
Maximum load @ −25 °C [W]	1000
Refrigerant Gas	R404A
Control System	
Typology	PLC
Serial interface	RS232
Remote control software	Winkratos 4
Security system (EUCAR 6)	Fire protection system H_2 Monitoring system Overpressure probe N_2 flux system N° 4 Pt100 thermoresistors

Moreover, as discussed in the introduction, some studies showed that the optimal operating parameters are linked to the PCM melting temperature chosen and therefore a cross-correlation analysis requires a parametric evaluation of the PCM melting point as well.

Facilities

The experimental equipment was chosen according to the battery

Table 4
Features of the Bitrode cycler used for testing.

| Main features	
Power	
Model	FTV-1 1000/100/10–20
Phases	3
Rated Operational AC Voltage	400 V
Frequency	50 Hz
Maximum AC AMPS	70 AMPS
DC Voltage Range	0–20 V (Res. 0.001 V)
Maximum DC Current	1000 A
Hardware	
N° of Channels	2
Maximum Data Acquisition Rate	0.1 s / Data Sample
Current Ranges Max	500 A (single channel) 1000 A (2 channel in parallel) (Res. 0.1 A)100 A (Res. 0.01 A)10 A (Res. 0.001 A)
Assignable Data Channel Inputs	2
Thermocouples Type	J
Temperature Range	−40 to 200 °C (Res. 0.5 °C)
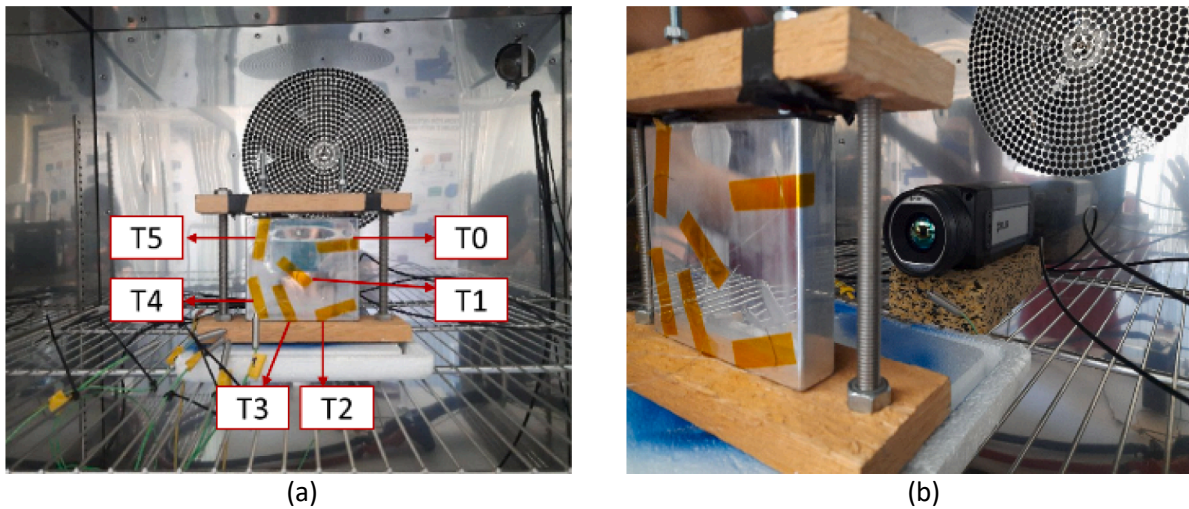
Fig. 2. Pictures of the battery placed inside the climatic chamber, showing a) a detail on the placement of the thermocouples, and b) a detail of the ir camera.

specifications and typology of tests.

Charging/discharging tests were carried out in humidity and temperature-controlled environment, to reproduce similar conditions to the operative cases and to fix clear references about surrounding ambient. An Angelantoni Discovery DM1600 BT climatic chamber (Temperature range: $-35\,°C$ - $+180\,°C$; Humidity range: $10 - 98\%$) with temperature precision of ±0.1 to 0.3 K has been used. The main features of the climatic chamber are summarized in Table 3. The temperature and the humidity inside the climatic chamber were monitored through Pt100 thermistors and a psychrometric system, respectively.

Control is achieved by means of a programmable logic controller (PLC) and is managed by a proprietary software (Mykratos). The charging/discharging cycles were achieved by means of a Bitrode cycler model FTV-1 programmed to realize all the procedures provided by the protocol schedule. The main features of the cycler are summarized in Table 4. The cycler is able to work with a voltage range of 0–20 V and can supply a value of ±500 A for each of its two channels. The channels are parallelable to reach an overall value of 1000 A, used in case of very high current rate tests. Current and voltage measurements of the cell were carried out via a voltage transformer and a current clamp and, internal to the cycler.

For the evaluation of the temperatures of the battery, two methods were used, temperature sensors and IR camera: the cell was equipped with six K-type, class A, thermocouples, as shown in Fig. 2, which were placed on the cell with thermal tape, including a layer of thermal paste for a better contact. The selected thermocouples have 0.25 mm diameter, which allows the fastest response time possible. At the same time, a FLIR A655sc IR camera was used to record the temperature evolution during the test and investigate surface temperature uniformity of the battery. Data from the temperature sensors were acquired using a National Instruments cDAQ system and a dedicated LabVIEW® software, whereas the data from the infrared (IR) camera were recorded using the proprietary software. Some pictures of the experimental setup are shown in Fig. 2.

Testing procedure

At first, tests were carried out to define the relation between the state of charge (SoC) and the open circuit voltage (OCV) at different temperatures, that was subsequently used for the implementation of the numerical model. To this aim, Hybrid Power Pulse Characterization (HPPC) tests were carried out to obtain detailed information on dynamic behaviour of the cell [64]. Table 5 describes the HPPC procedure implemented.

Table 5
HPPC test protocol.

HPPC Test (Hybrid Power Pulse Characterization)				
Step	Phase	Parameters	Stop Criteria	Loop
1	Start condition	Thermally stable (3 temperatures, 25, 35 and 45 °C) and fully charged	–	
2	Discharge	T; V; I (3C)	$V \leq 1.5$ V $\parallel$ t > 10 sec	Repeat N times until fully discharged
3	Rest	–	t = 1 min	
4	Charge	T; V; I (3C)	$V \geq 2.7$ V $\parallel$ t > 10 sec	
5	Rest	–	t = 1 min	
6	Discharge	T; V; I (1C)	$V \leq 1.5$ V $\parallel$ $Cap_{disch} \geq X\%$	
7	Rest	–	t = 2 h	
8	Galvanostatic Charge	T; V; I = 1C	$V \geq 2.7$ V	
9	Potentiostatic Charge	T; I; V = 2.7 V	$I \leq 0.1$ A	
10	Rest	–	t = 2 h	

*the capacity reduction selected for each step depends on the SoC working window: from 100% to 90% and from 10% to 0% a capacity reduction of 1% is performed while from 90% to 10% this value increase to 5%. This is done to obtain a better fitting in high variability zones such as fully charge and complete battery discharge.

Symmetric high C-rate discharge and charge pulses (3C) were performed at each step. The C-rate is a measure of the rate at which a battery is discharged relative to its maximum capacity [65,66]. Each constant current discharge phase was stopped when the lowest cell voltage reached the threshold value of 1.5 V. Instead, each constant current charge phase was stopped when the highest cell voltage reached the threshold value of 2.7 V. This value corresponds to a SoC of 100%. Once the fully charged condition was reached, a partial discharge (a percentage of total capacity) of the battery was performed at constant voltage to move the system in another SoC point. A long rest phase is then applied to evaluate the OCV at a very stable condition. The relationship between SoC and OCV can be extracted in this way. Before the beginning of each test, the cell was subjected to a thermal conditioning phase at 25 °C in the climatic chamber. The initial charge pulse was initialized when the temperature of the cell reached the set-point value

Table 6
Different c-rates test protocol.

Step	Phase	Parameters	Stop Criteria	Loop
	Different C- Rates Test			
1	Start condition	Thermally stable (25 °C) and fully charged	–	–
2	Discharge	T; V; I (1C, 2C, 3C, 4C)	V ≤ 1.5 V	Repeat for various C-rates
3	Rest	–	t = 2 h	
4	Galvanostatic Charge	T; V; I (1C, 2C, 3C, 4C)	V ≥ 2.7 V	
5	Potentiostatic Charge	T; I; V = 2.7 V	I ≤ 0.1 A	
6	Rest	–	t = 2 h	

of 25 °C.

Subsequently, dedicated tests to define the thermal behaviour of the battery under different operating conditions (charge/discharge) were performed as follows: the cell was fully charged at constant current until the voltage reached a value corresponding to the upper cut-off voltage (2.7 V); then the current was gradually reduced until 0.1 A while maintaining the voltage reached (upper cut-off). The combination of galvanostatic and potentiostatic phases was adopted, which is normally used to fully charge a battery (100% SoC) [67]. Finally, the cell was deep discharged at constant current until the lower cutoff voltage (1.5 V). During the tests, climatic parameters were monitored and controlled with the climatic chamber set at 25 °C and all the steps were performed sequentially. The following C-rates were selected both in charge and discharge: 1C, 2C, 3C, and 4C corresponding respectively to 23, 46, 69, and 92 A. The charge and discharge C-rates start from 1C (23A) and reach progressively (with increment of 1C) the value of 4C (92A) (see Table 6). This high C-rate value is allowed by the particular technology used which consents very stable conditions not only at high C-rate in discharge but also in charge, usually a critical situation for lithium battery with graphite anode due to lithium plating phenomenon [68]. Also, a very high depth of discharge (DoD) is guaranteed without significant impact on lifetime, as declared by the producer.

The experimental error on the temperature measurement is in the range of ± 0.3° C according to the datasheet of the producer whereas the instrumental error for voltage and current is within 5% as declared by the producer of the cycler. Therefore, the experimental results shown in Section 3.4 are affected by negligible errors and are highly reproducible.

Results

Electrical characterization of the cell

Results from the Hybrid Power Pulse Characterization tests were used to obtain the SoC-OCV relation and the dynamic response of the battery to charge and discharge pulses.

The SoC was calculated starting from the measured voltage and current based on the Coulomb counting algorithm. It can be considered as the ratio between the available capacity $\Delta - Cap_{av}$ [Ah] and the nominal one Cap_n[Ah], which is reported in Table 1 [69]:

$$SoC = SoC_0 + \frac{\Delta Cap_{av}}{Cap_n}.100 \tag{1}$$

$$\Delta Cap_{av} = \int_0^\tau i(t)dt. \tag{2}$$

where SoC_0 is the initial state of charge, i(t) is the current measured at time t [A] and τ [h] is the total duration of the charge/discharge process.

The SoC-OCV curve is extremely important for algorithms used to determine the variable SoC value and to know relaxing behaviour, while the response to short charge and discharge pulses can help extraction of circuital models able to fit the dynamic behaviour of this kind of electrochemical storage devices. Due to the temperature dependency of the SoC-OCV relationship, the tests were performed at three different working temperatures (25, 35 and 45° C respectively) to evaluate the influence of this parameter on the battery response. The complete test carried out at 25 °C in a climatic chamber for environmental control is shown in Fig. 3, while Fig. 4 reports the typical response to a defined SoC step. In particular, it shows the two charge and discharge pulses at high C-rate (3C) and the consequent voltage response; these steps, interspersed with short (1 min) rest phases, useful for OCV extraction, are followed by the capacity reduction step, which brings the battery to the next SoC value. SoC steps in the test were done with a variation of 1% between 10% and 0% and between 100% and 90%, since in these ranges there is a strong variation of the SoC-OCV curve. In the remaining range,
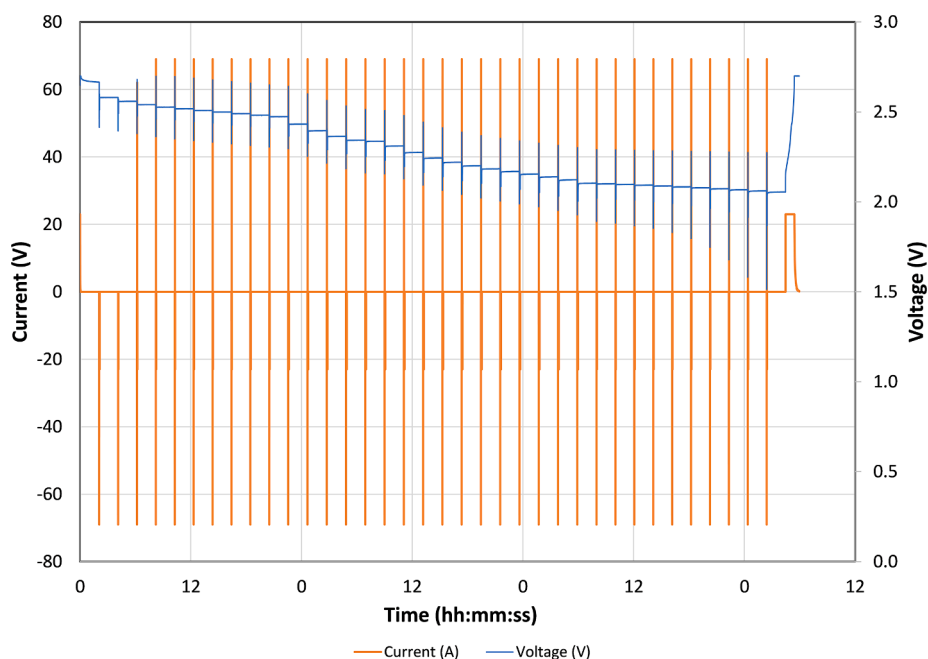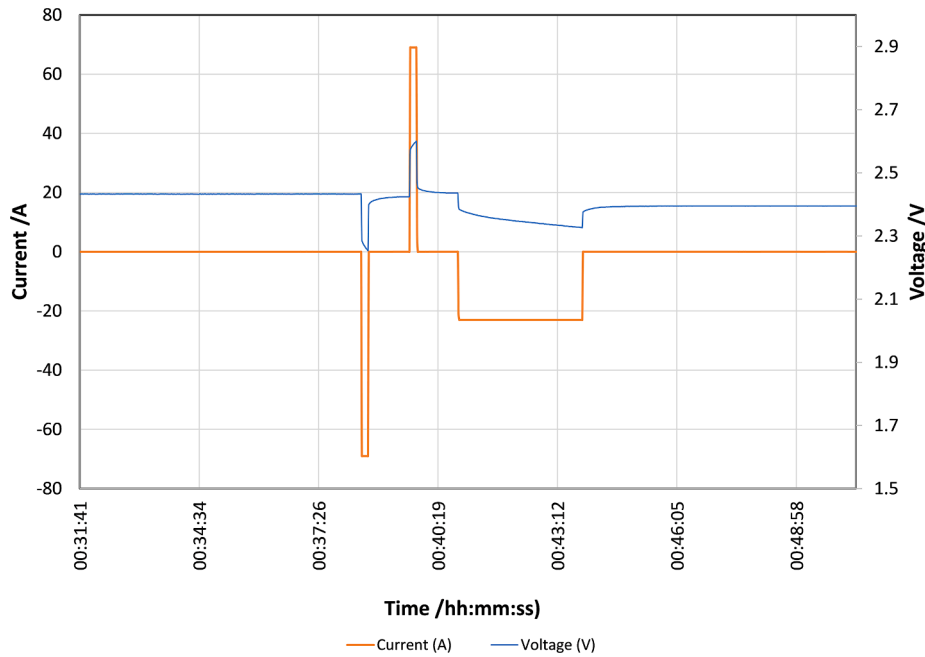

Fig. 3. HPPC test: Voltage and Current vs Time.

Fig. 4. HPPC test: zoomed view of Voltage and Current vs Time at a specific value of SoC.
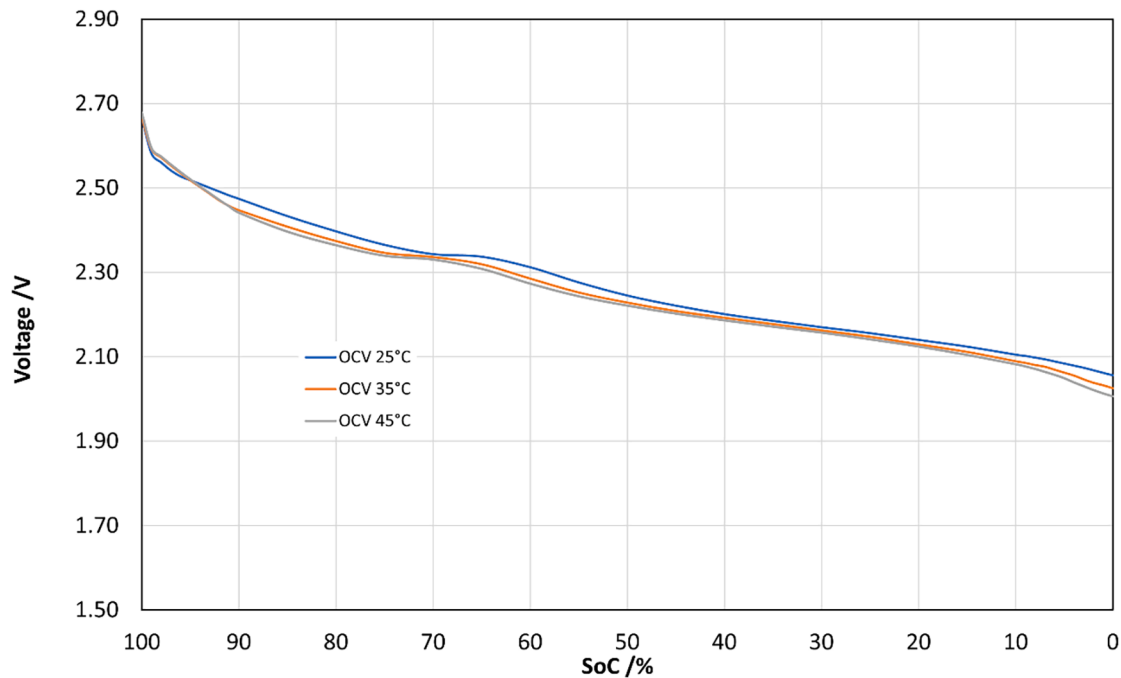

Fig. 5. SoC-OCV curves at various temperatures.

the variations considered were 5% between one step and the following. The SoC-OCV curves at various temperatures are reported in Fig. 5. There are small differences between the various temperatures, especially visible around the 70% SoC, where the typical "hump" of the LTO battery curve occurs. This is normally associated to a phase change of the cathode [70] and tests show it inclined to move to higher SoC with increasing temperature; also a higher reduction of the voltage happens with increasing temperatures.

The temporal trends of voltage and current for the test at various C-rates in charge and discharge are reported in Fig. 6, while the typical discharge curves at various C-rates vs the discharged capacity are visible in Fig. 7. This graph shows a little reduction of the capacity extracted in

case of using the standard discharge current value (23 A) or the higher ones. Also, for the 2C, 3C and 4C currents, the capacity discharged is practically the same, enhancing the good quality response with high C-rate values. Numerically, the capacity discharged is about 23,32 in the first case (23 A) while the value settles around 23,1 in the other cases, showing a reduction of only the 0,1%.

Thermal characterization of the cell

The aim of the thermal characterization of the cell was to evaluate the sensitivity to the charge/discharge rate in terms of the maximum temperature reached, the average temperature from the 6 installed sensors and the temperature uniformity of the cell:
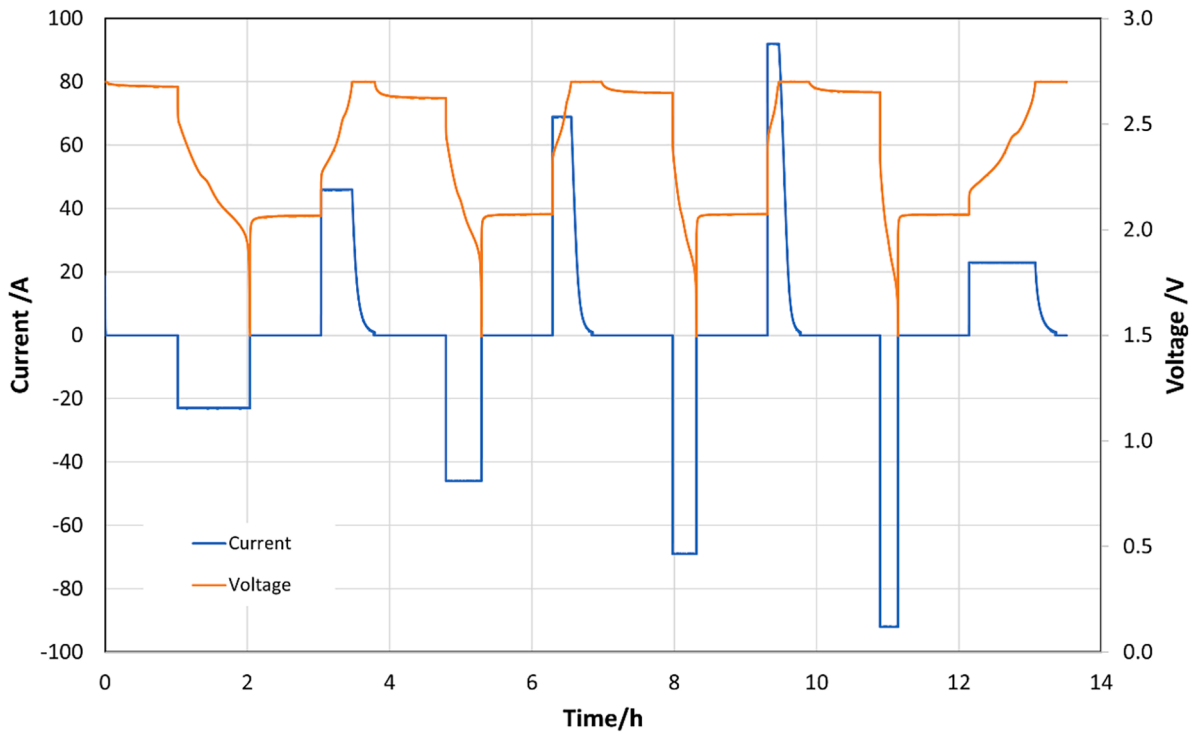
Fig. 6. Various c-rate charge and discharge test: voltage and current vs time.
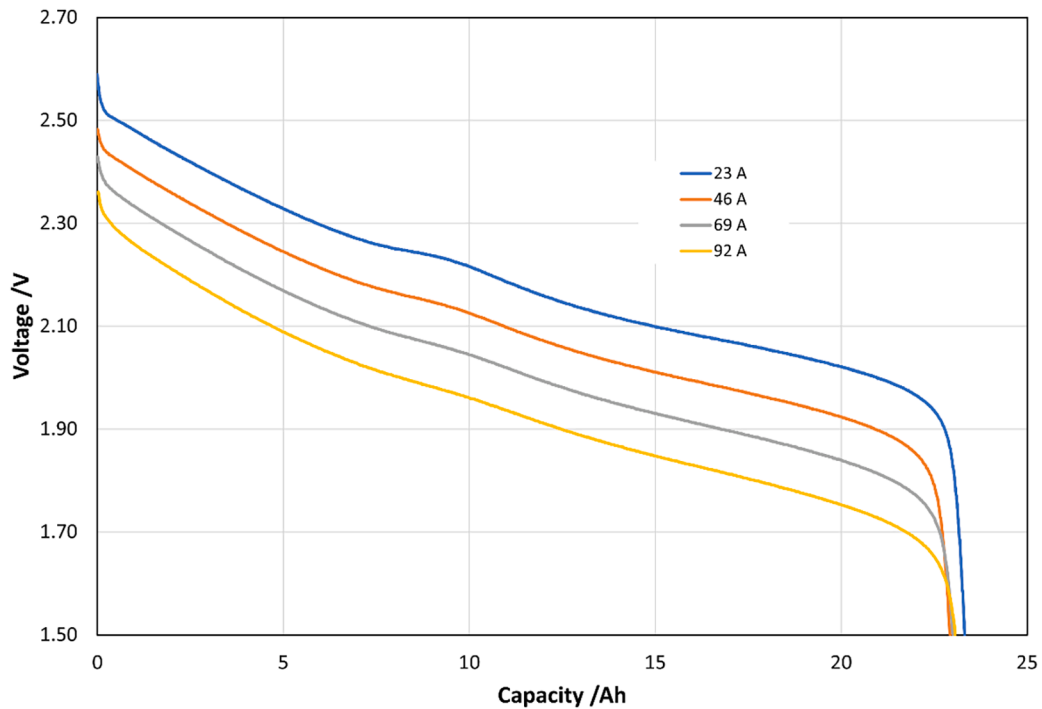

Fig. 7. Discharge voltage vs capacity at various c-rates.

$$\Delta T_{max} = T_{max} - T_{min} \tag{3}$$

where T [k] is the temperature measured by the sensors installed on the cell.

The temperatures measured during the test at 25 °C with the current/voltage conditions from Fig. 6, are reported in Fig. 8. As it is possible to notice, there is a clear effect of the C-rate on the heating up of the cell and, more specifically, while for 23 A, the max temperature reached by

the cell does not exceed 30 °C, for the charge at 4C a maximum temperature of 42 °C is measured. Heating occurring during discharge is slightly more marked than during charge.

Fig. 8 shows that the temperature uniformity on the cell is good and the only significant deviation measured is that of T3. This result is due to an imperfect contact of the sensor with the cell. The maximum temperature measured by the camera during the charges/discharges are in line with the temperatures measured by the thermocouples, whose
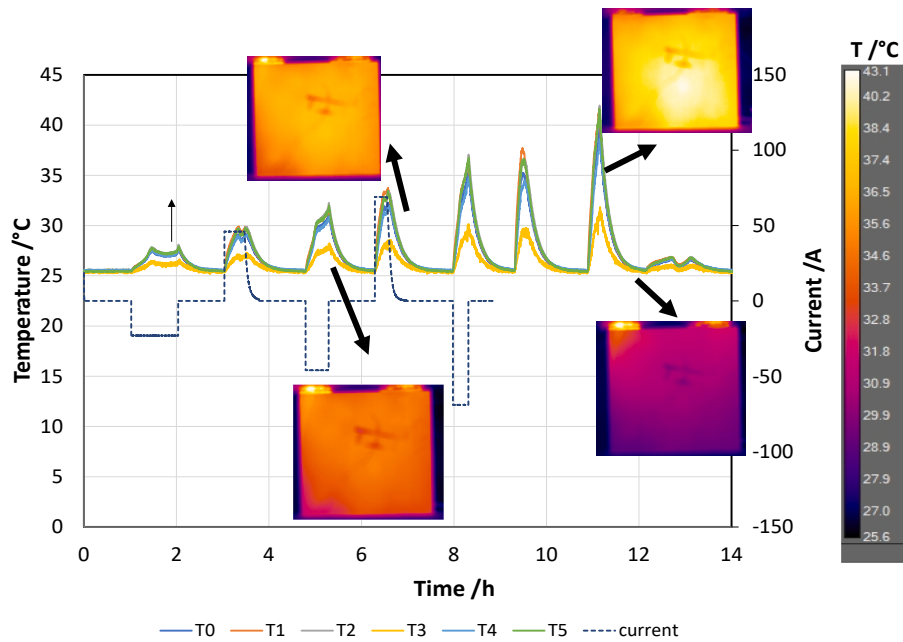
Fig. 8. Temperature and current profiles at 25 °C ambient temperature different charge–discharge cycles. The four insets are instantaneous IR photographs showing the temperature distribution on the battery.
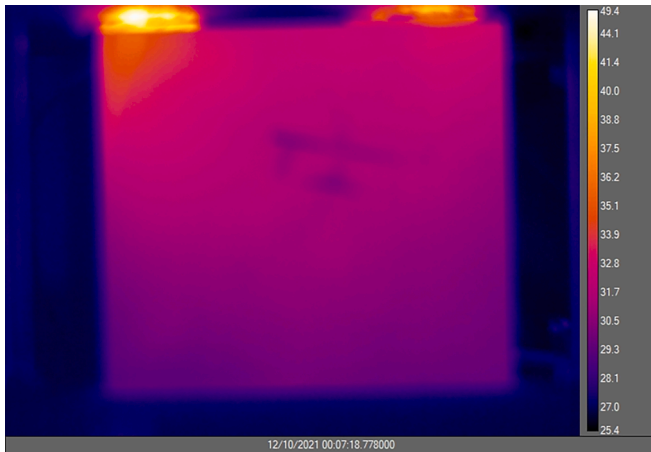

Fig. 9. Example of temperature maps from the ir camera.

values were then considered for the model validation. It is worth noticing that, as shown in a sample picture from IR camera in Fig. 9, the temperature of the electrodes of the battery is much higher than in the rest of the cell, especially during the charge/discharge at high C-rate (up to 6 K higher). This effect was however not considered in the numerical model, since the aim of the TMS is to limit and make more uniform the surface temperature of the cell.

The main highlights from the thermal tests are as follows:

- The temperature difference among the different points of the surface of the cell is within 1 K, thus indicating a good uniformity;
- The maximum temperature on the cell varies from 30 °C to 42 °C passing from 23 A to 90 A during discharge;
- There is a slight difference in the thermal behaviour of the system from charge to discharge cases, with the charging process resulting in higher heating of the cell for lower rates and the discharging process accounting for higher heating of the cell at higher rates. Such a behaviour is already documented in the literature [16,71,72] and depends on the different processes that dominate the charge and

discharge of the system. For the implementation of the numerical model, the heat generation is considered the same for the charge and discharge; however, a correction factor to take into account the different heat dissipation towards the ambient was introduced as a function of temperature, as will be discussed in section 4.1.

Heat generation

Heat generation in batteries is due to several phenomena occurring as a result of electrochemical reactions taking place during charging/discharging cycles. It can be calculated with equation of Bernardi et. al. [73]:

$$Q_c = i_c(OCV - V_c) - i_c T \frac{d(OCV)}{dT} \tag{4}$$

where i is the current flow across the cell [A] (<0 discharge mode, >0 charge mode, $=0$ open circuit mode), OCV is the equilibrium potential or open circuit voltage [V], V is the cell voltage [V], T is the absolute temperature [K].The subscript c stands for cell.

Q_c is usually decomposed in an irreversible component $Q_{c,irr}$ owing to Joule dissipation and a reversible component $Q_{c,rev}$ generated by entropy changes. Q_{irrev} is always positive while Q_{rev} can be either positive or negative. Their expressions are:

$$Q_{c,irr} = i_c(OCV - V_c) \tag{5}$$

$$Q_{c,rev} = i_c T \frac{d(OCV)}{dT} \tag{6}$$

The heat generated was calculated and is reported in Fig. 10. The following considerations can be done:

- The heat generated ranges from 10 to 90 kW/m^3, which is in line with the results reported in [13].
- The heat increases with the current for charge/discharge, as expected. However, the increment is not linear, since passing from 1C to 4C, the heat generated increases by a factor 9.
- At lower currents, there is not significant difference between the charging and discharging process, however for the case of 4C the discharging process induces higher heat generation. Such a situation is discussed in [71] and is connected to the different phenomena
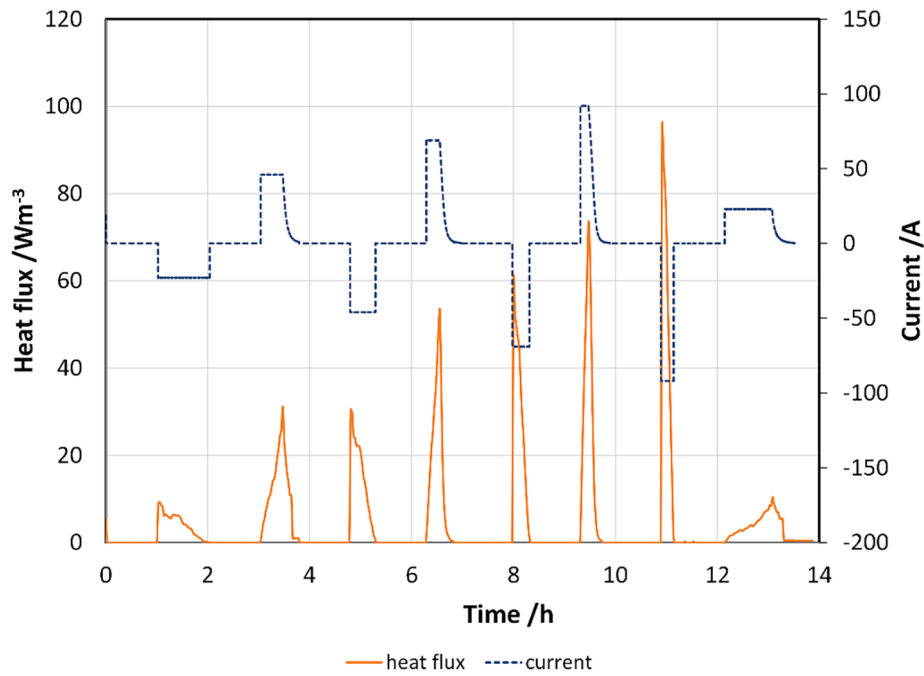
Fig. 10. Heat generated during the test reported in Fig. 7.

Table 7
Thermal proprieties of the casing and cooling plate materials.

	Casing	Plate
Density [kg/m^3]	1991	2700
Specific heat capacity [kJ/(kg/K)]	2138	900
Thermal conductivity [W/(m K)]	200	238

(a) Naturally air-cooled cell

(b) Passive PCM-based cell cooling

casing
PCM
cooling plate

(c) Passive hybrid PCM+water cell cooling

Fig. 11. Cell geometries implemented in comsol.

dominating the two processes for Li-ion batteries. In particular, according to the authors in [71], the dominant phenomenon during charge is the polarization heat of negative electrode, while the during discharge is the polarization heat of positive electrode. This indicates that, in case of high-current applications, the discharge process is the most severe one for the thermal generation of the battery. Accordingly, in the next sections, the discharge current will be used as a reference parameter for the evaluation of the effect of operating conditions on the behaviour of the battery.

Such results represent the basis for the following optimization activity.

Numerical model

A 3D physical model of the system was implemented in the Finite Element software COMSOL Multiphysics®. The simulated battery is a prismatic cell of dimensions 106 mm × 116 mm × 22 mm (Table 1). The thermal properties of the PCMs are reported in Table 2 whereas the properties of the casing of the cell and of the cooling plate are reported in Table 7. These properties together with the measured data of voltage and current sampled were used as inputs of the model. The maximum temperature reached by the cell was selected as outcome to discuss and compare the results.

The model was validated against the experimental results discussed in Section 3.4 regarding the naturally air-cooled cell (Fig. 11 a). Then the model was used to perform a parametric analysis on two cooling TMSs: a PCM-based and a hybrid PCM + water cooling. In the PCM-based system the cell is in contact with a PCM layer placed on the two wider external surfaces of the casing, as shown in Fig. 11b. The PCM was placed in such a configuration to enhance the uniformity of the cell temperature. The hybrid system is the same passive TMS with an additional channel with cooling water flowing upwards through an aluminium plate for each PCM layer, as shown in Fig. 11c.

The following modelling assumptions were made:

- Physical properties of the materials constant with temperature variations;
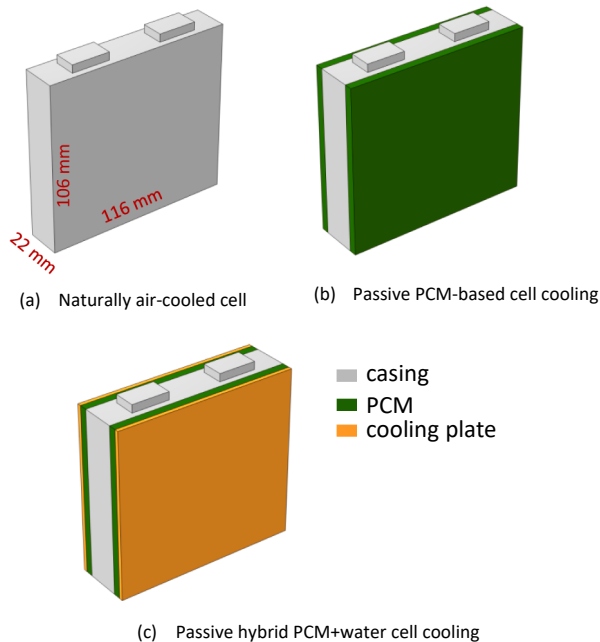- Negligible heat exchange by radiation on the outside of the cell;

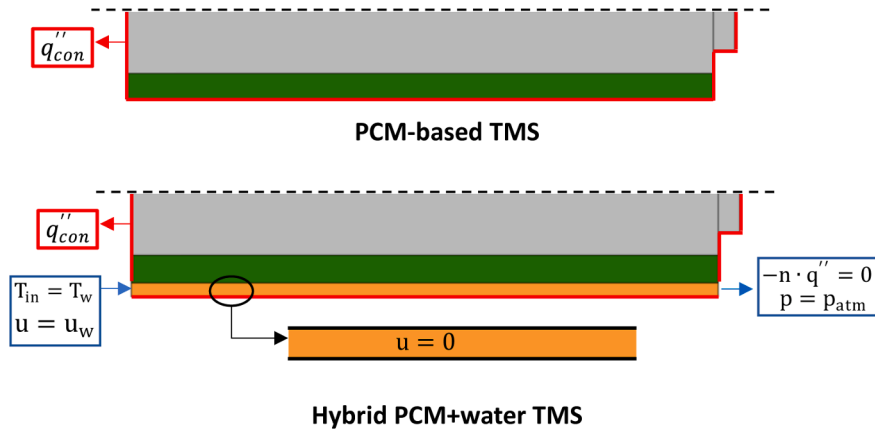**PCM-based TMS**

Hybrid PCM+water TMS

Fig. 12. Boundary conditions assumed in the simulations. Due to the symmetry of the geometry only half computational 2d domain is shown. In the surfaces parallel to the section shown were assumed the same Neumann and no slip boundary conditions.
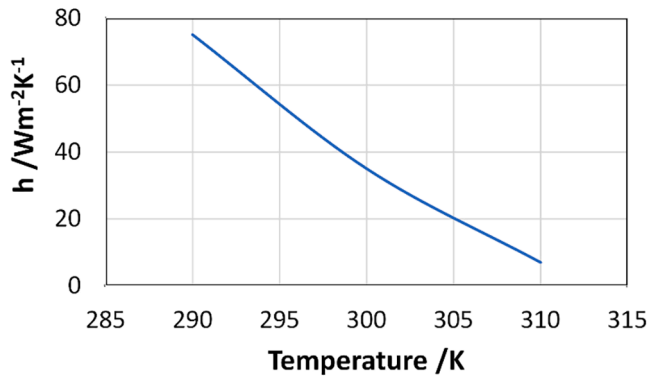

Fig. 13. Temperature dependence of the convective coefficient for the fluid/battery interface.

- Negligible convective heat transfer at the interface solid–liquid of the PCM;
- Negligible thermal contact resistance between two different layers;
- Uniform thermal dissipation of the cell;
- Heat dissipated by the cell during charging/discharging cycles applied as volumetric heat source to the cell domain;
- Newtonian flow inside the cooling plate.

During the experimental campaign described in Section 3.3 the battery exhibited OCV hysteresis, i.e. the cell voltage during the discharge process was lower than the one during charge process. The detailed description of the thermodynamic entropic effects, mechanical stress, and microscopic distortions within the active electrode materials causing the OCV hysteresis is out the aim of this paper, so that the developed thermal model ignores this phenomenon. However, this assumption does not significantly influence the results, as demonstrated by the model validation in section 4.2.

The following boundary conditions of which the first one applied only to the passive PCM-based TMS were assumed (Fig. 13):

- Natural convective heat transfer on the external surfaces (Neumann's condition). q''_{con}
- Inlet temperature of the water ($T_{in} = T_w$);
- Adiabatic condition at the outlet boundary ($-n \bullet q'' = 0$);
- Inlet velocity of the water ($u = u_w$);
- Newtonian fluid and no slip conditions on the walls in contact with the fluid;

- Pressure condition of static relative pressure at 0 Pa at the outlet boundary ($p = p_{atm}$).

The convective flux q''_{con} [W/m^2] on the external surfaces is given by Newton's law:

$$q''_{con} = h\,(T_s - T_{air}) \tag{7}$$

where h is the heat transfer convection coefficient [W/(m^2 K)], T_s is the temperature of external surface in contact with the fluid [K] and T_{air} is the temperature of external air.

The model was tuned setting up the h value to fit the experimental data. In particular, h was implemented as function of the temperature as shown in Fig. 13. In this way it is possible to take into account the variation of the effective thermal conductivity of the battery according not only to the operating conditions but also to the hysteresis in charge/discharge [14].

Numerical simulations were performed in transient condition and all domains are initially started at the same ambient temperature monitored during the experimental test. Moreover, for the hybrid system initial velocity of water was set to 0 m/s whereas initial temperature of the water was equal to T_w.

All simulations were carried out with a triangular adaptive mesh with minimum and maximum element size of 1 0.464 and 6.38 mm, respectively. The curvature factor and the maximum element growth rate are 0.4 and 1.4, respectively. As the accuracy of the simulations is affected by the mesh size, a grid dependency analysis was carried out aiming at minimizing the discrepancy between exact and approximated solution. The criterion to select the grid (~50 k elements) for the final simulations was an average discrepancy below 2 % in the predicted values of the average surface temperature of the cell.

Mathematical equations

The conduction heat transfer mechanism occurring across the i-th solid domain (Fig. 11) can be expressed by means of Fourier's law [74]:

$$\rho_i\,cp_i\frac{\partial T}{\partial t} = k_i \nabla^2 T + q''_i \tag{8}$$

where ρ is the density [kg/m^3], cp the specific heat [kJ/(Kg K)], k the thermal conductivity [W/(m K)], q''' the volumetric heat source [W/m^3].

The volumetric heat source in the active part of the battery was evaluated as follows:

$$q''_b = \frac{Q_c}{Vol_c} \tag{9}$$

where *Vol* the volume of the cell [m^3], and the subscript b stands for battery. Q_c is the term associated to heat generation during charge/discharge, that was discussed in section 3.4.3.

The energy balance equations for the PCM can be expressed as follows [75]:

$$\rho_{PCM} \frac{\partial H}{\partial t} = k_{PCM} \nabla^2 T \tag{10}$$

where H is the overall heat capacity of the material [J/kg], that can be expressed as:

$$H = \int_{T_0}^{T} cp_{PCM} dT + \alpha\beta \tag{11}$$

where T_0 is the initial temperature, α is the liquid fraction of the PCM, β is the specific phase change enthalpy [J/kg]. In turn, α is defined as:

$$\alpha = \begin{cases} 0 \, (T < T_{cr}) \\ \dfrac{T - T_{cr}}{T_{mel} - T_{cr}} \quad (T_{cr} < T < T_{mel}) \\ 1 \, (T > T_{mel}) \end{cases} \tag{12}$$

where T_{cr} is the crystallisation temperature of PCM and T_{mel} is the melting temperature of PCM. In the hybrid TMS the mass fluid enters and leaves the control volume through a mechanism referred as advection. The flow motion can be described through Navier-Stokes and continuity equations. These based on 3D space rectangular coordinate system, can be expressed as follows [74]:

$$\rho_f \frac{\partial \vec{u}}{\partial t} + \rho_f (\vec{u} \bullet \nabla)\vec{u} = \rho_f \vec{g} - \nabla p + \mu_f \bullet \nabla^2 \vec{u} \tag{13}$$

$$\rho_f \nabla \vec{u} = 0 \tag{14}$$

where $\vec{u}$ is the vector velocity of the fluid (m/s), p the pressure (Pa), g the gravity acceleration (m/s^2) and μ the coefficient of dynamic viscosity (Pa s), and the subscript f stands for fluid.

To know the flow regime the Reynolds number was calculated as follows [74]:

$$Re = \frac{\rho_f u D_{eq}}{\mu_f} \tag{15}$$

where D_{eq} is the equivalent diameter [mm].

Model validation

The model was validated against the experimental data previously discussed. In detail, the simulated and experimentally measured average temperature of the cell were compared, as shown in Fig. 14. Overall, the simulation results showed good agreement with the experimental data.

It is worth noticing that the difference between the model prediction and the measured data is more marked during the cooling phase of the battery. However, the average deviation between the experimental and simulated temperatures is always lower than 2 K, i.e., lower than 10%., which points out the ability of the model of describing the operation of the battery.

The numerical results were further validated via the statistical metric mean bias error (MBE %) and root mean square error (RMSE %) calculated as follows:

$$MBE\% = \frac{\sum_{i=1}^{N}(T_{i,m} - T_{i,ex})}{N \bullet T_{av,ex}} \bullet 100 \tag{16}$$

$$RMSE\% = \left[\frac{\sum_{i=1}^{N}(T_{i,m} - T_{i,ex})^2}{N} \right]^{0.5} \bullet \frac{100}{T_{av,ex}} \tag{17}$$

where $T_{i,m}$ is the ith value predicted by the model, $T_{i,ex}$ is the ith measured experimental value, $T_{av,ex}$ is the experimental mean value and N is the total number of measurements.

Based on the results, MBE % (0.9) and RMSE % (4.3), the model can be actually considered a good representation of the experimental data.

Numerical results

The validated model was used to carry out parametric simulations to identify the influence of operating conditions and design parameters of a battery equipped with a passive cooling thermal management system. This section was divided into two subsections. In the first section the influence on the thermal behaviour of a PCM-based system was discussed aiming at investigating the effect of (i) ambient temperature T_{amb}, (II) discharge current I_d, (III) PCM layer thickness s, and (IV) phase change temperature T_{pc}. In the second section the influence on the thermal behaviour of a hybrid PCM + water system was discussed aiming at investigating the effect of (i) temperature of the cooling water T_w, (ii) velocity of the water inside the cooling channel u_w, and (iii) thickness of the cooling plate $s_{channel}$. It is worth noticing that conditions not commonly evaluated – and that might instead represent significant
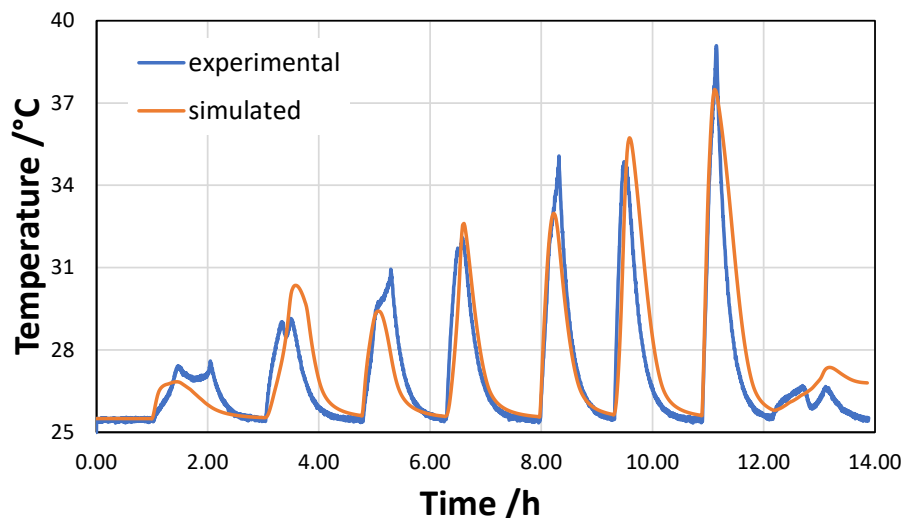

Fig. 14. Comparison between measured and simulated temperature profiles. The experimental temperature plotted is the average temperature of the six thermocouples used during the charging/discharging tests (Fig. 8).

stress factors for the cells – are taken into account. Simulations of the hybrid system were performed by starting from the optimal design of the PCM-based TMS.

In order to reduce the number of simulations needed for the evaluation of the effect of such parameters, Taguchi methods was used for the design of experiment. It is considered a powerful tool for designing high quality systems [62]. According to the common language used in the context of the Taguchi method, variable parameters to investigate and their values are referred to as "Factors" and "Levels", respectively. The method is based on the evaluation of an orthogonal array with the characteristic that, for each level of a particular parameter, all L levels of each of the (P-1) other parameters are tested at least once. It avoids the simulation of all L^F possible combinations [76].

PCM-based TMS

For each of the factors T_{amb}, I_d, s, T_{pc}, four levels were considered, as shown in Table 8. Regarding the phase change temperature, this was considered as the average between the melting and crystallization temperatures of the selected PCMs according to the producer datasheets, with the exception of the 40 °C case, as discussed in section 3.1. It is worth noticing that the selected levels for the PCM thickness are quite large compared to the overall battery size. However, as previously discussed, two of the main issues considered in the present work and that are not commonly considered in the literature analysis are the fast charging/discharging of these batteries, and the operation upon multiple fast charge/discharge cycles. This is specifically due to the foreseen application in hybrid battery systems or in cases where extremely fast charge/discharge and several continuous cycles are needed. Accordingly, the amount of heat released is high and requires a high volume fraction of PCM. So the main aim of the work is to present a design methodology, a dedicated analysis for space reduction can be done following the same procedure to further improve the TMS.

L₁₆ orthogonal array

In this work, by using the Taguchi method, the number of simulations was significantly reduced, from $4^4 = 256$ to 16 cases. The detailed L_{16} orthogonal array generated in MATLAB software and indicating all the simulated combinations is shown in Table 9.

The maximum temperature reached by the cell and the temperature uniformity allow to evaluate the thermal behaviour of the cell. However, as highlighted from experimental results, the temperature uniformity of the cell is always good and only minor differences are reported. Hence, for the present analysis, the maximum temperature was selected as suitable indicator to evaluate the effect of the factors in the 16 simulations carried out. Results are shown in Fig. 15. According to the model results, the maximum temperature values exhibited by cases 15 and 16, 63.12 °C and 71.39 °C, respectively are well above the optimal range of safe temperature for Li-ion cells, typically 20–60 °C [77,78]. Therefore, the battery operation under the operating conditions of these test cases should be avoided to prevent severe issues of thermal runaway. As shown in Table 9, these critical conditions occurred at high values of air temperature (45 °C) and/or discharge current (69-92A). In contrast, case 1 (27.58 °C) represents the best operative condition to guarantee the thermal safety of the battery.

In addition to the simulated cases, the results from experimental

Table 8
factors and levels selected for the numerical simulations of the PCM-based TMS.

Levels (L)	Factors (F)			
	T_{amb} [°C]	I_d [A]	s [mm]	T_{pc} [°C]
1	25	23	5	32
2	30	46	10	36
3	35	69	15	40
4	45	92	20	46

Table 9
Taguchi orthogonal array for the numerical simulations of the PCM-based TMS.

Simulation	T_{amb} [°C]	I_d [A]	s [mm]	T_{pc} [°C]
1	25	23	5	32
2	25	46	10	36
3	25	69	15	40
4	25	92	20	46
5	30	23	10	40
6	30	46	5	46
7	30	69	20	32
8	30	92	15	36
9	35	23	15	46
10	35	46	20	40
11	35	69	5	36
12	35	92	10	32
13	45	23	20	36
14	45	46	15	32
15	45	69	10	46
16	45	92	5	40

activity on the cell without any TMS at 25 °C and 45 °C ambient temperature are reported. The highest maximum temperature, ~76 °C, is exhibited by the cell without any TMS at 45 °C. It can be noted that the PCM is proven to be an efficient thermal management system. In detail, at 45 °C and 92 A, a 5 mm thick PCM layer with transition temperature 40 °C (case 16) reduces the maximum temperature by 4.61 °C. At 25 °C and 92 A, a 20 mm thick PCM layer with transition temperature of 46 °C (case 4) reduces the maximum temperature by 5.11 °C.

Fig. 16 shows the effect on the level-averaged maximum temperature of the four selected factors. The prediction of the Taguchi method shows that the maximum cell temperature increases sharply with increasing T_{amb} and I_d values. In contrast, in the tested conditions the effects of the thickness of the PCM and its phase change temperature are less marked. Taken 60 °C as the upper limit of the cell temperature, the values recommended are T_{amb} below 45 °C (level 4), I_d below 69 A (level 3), s above 10 mm (level 2), and T_{mel} above 40 °C (level 3).

As an example, Fig. 17 reports the temporal trend of the average temperature of the cell for all the simulations, classified according to the ambient temperature. For each ambient temperature, the average temperature of the cell increases with the discharging current, that is increasing passing from simulation 1 (23 A) to simulation 4 (92 A), from simulation 5 (23 A) to simulation 8 (92 A), from simulation 9 (23 A) to simulation 12 (92 A) and from simulation 13 (23 A) to simulation 16 (92 A). However, from the picture, it is also possible to derive that there is a complex interaction between all selected factors, which is highlighted by the irregular trend of the average temperature of the cell predicted. For instance, while at T_{amb} 25 °C the cell reached its maximum temperature within the first hour of the cycle for all the simulation, at 35 °C this is achieved only after 2 h. Moreover, for the higher ambient temperature, the difference in the maximum temperature reached by the cell in the various simulations increases, passing from 10 K at 25 °C to 23 K at 45 °C. Such results indicate that it is not possible to analyse separately the influence of each parameter, but rather a more complex analysis is needed.

Interaction matrix

From what discussed in the previous section, it follows that the results reported in Fig. 16 can give only partial indications for the optimal design of the TMS. The interaction plots shown in Fig. 18 highlight that there is a strong dependence among the various selected factors. Each graph in the ij cell of the obtained matrix represents the i parameter as series and the j as abscissa.

For example, the blue line on the graph given by the intersection between the first row and the second column represents the parametric simulations carried out at ambient temperature of 25 °C for the four selected discharge currents (the four markers on each curve). Similarly, the blue line on the plot given by the intersection between the second
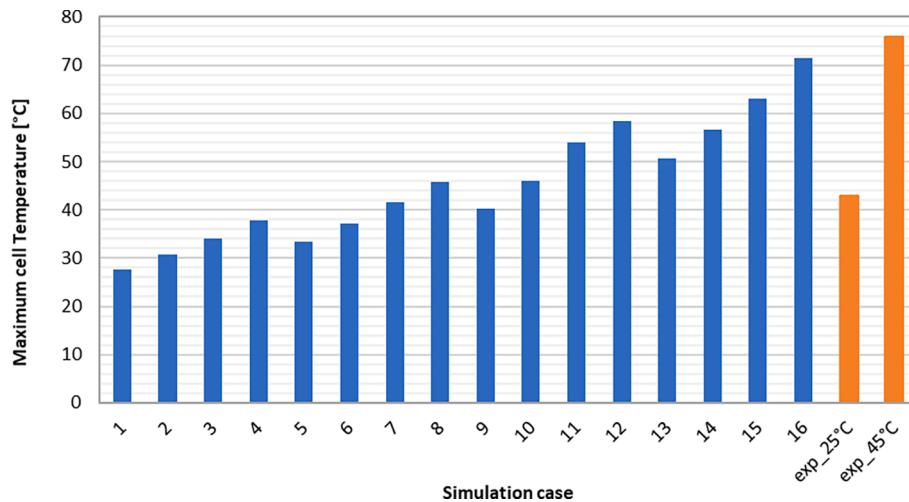
Fig. 15. Maximum cell temperature predicted for the selected 16 simulations. Orange data bars refer to experimental conditions of the cell without any tms at 25 °C and 45 °C for 92 A discharge current. (For interpretation of the references to colour in this figure legend, the reader is referred to the web version of this article.)
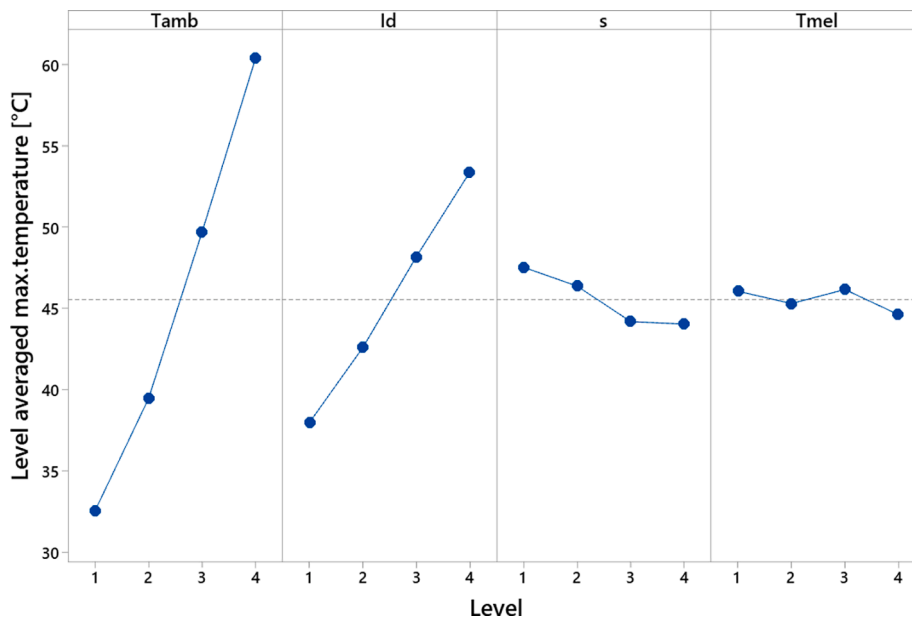

Fig. 16. Predicted effect of factors on the maximum cell temperature.

row and the first column represents the parametric simulations carried out at discharge current of 23 A for the four selected ambient temperatures. The tags in each point of the plot indicate the number of the simulation considered for that specific point, according to the list in Table 9.

From the interaction plot, the following discussion points arise:

- The effect of ambient temperature is clear and does not change for the various parameters: by increasing ambient temperature there is always an increase in the maximum temperature reached by the cell.
- For each ambient temperature considered, changing the thickness of the PCM or its melting temperature, does not significantly affect the maximum temperature reached by the cell.
- The effect of the discharge current is more marked for the smaller thickness of PCM (5 and 10 mm) whereas it affects less the maximum temperature reached for the higher thicknesses of PCM. This is due to higher inertia achieved in this case, and this also indicates that, if operation under very high currents is foreseen, increasing the thickness of the PCM might be a viable strategy.

- a higher melting temperature of the PCM is beneficial, especially at higher discharge rates and in combination with a higher thickness of the PCM. Indeed, in this way, if prolonged usage is foreseen at higher currents, due to the low thermal conductivity of the PCM, the time needed to complete the phase change increases and therefore it is possible to keep the temperature below the safe limit for a longer period.

Optimal design

In order to complete the analysis of design and operating parameters carried out so far, a parametric optimization was considered. The favourable values of each factor can be evaluated according to the S/N ratio, which is the ratio between the level of a desired signal to the level of the background noise. In this case, the signal is presented by the desired value, whereas the noise represents the undesired conditions. According to the S/N parameter, the performance index of each configuration can be evaluated considering three cases: smaller the better (SB), nominal the better (NB) and larger the better (LB) [79]. In this case, the mean value of the S/N ratio was defined so that the higher
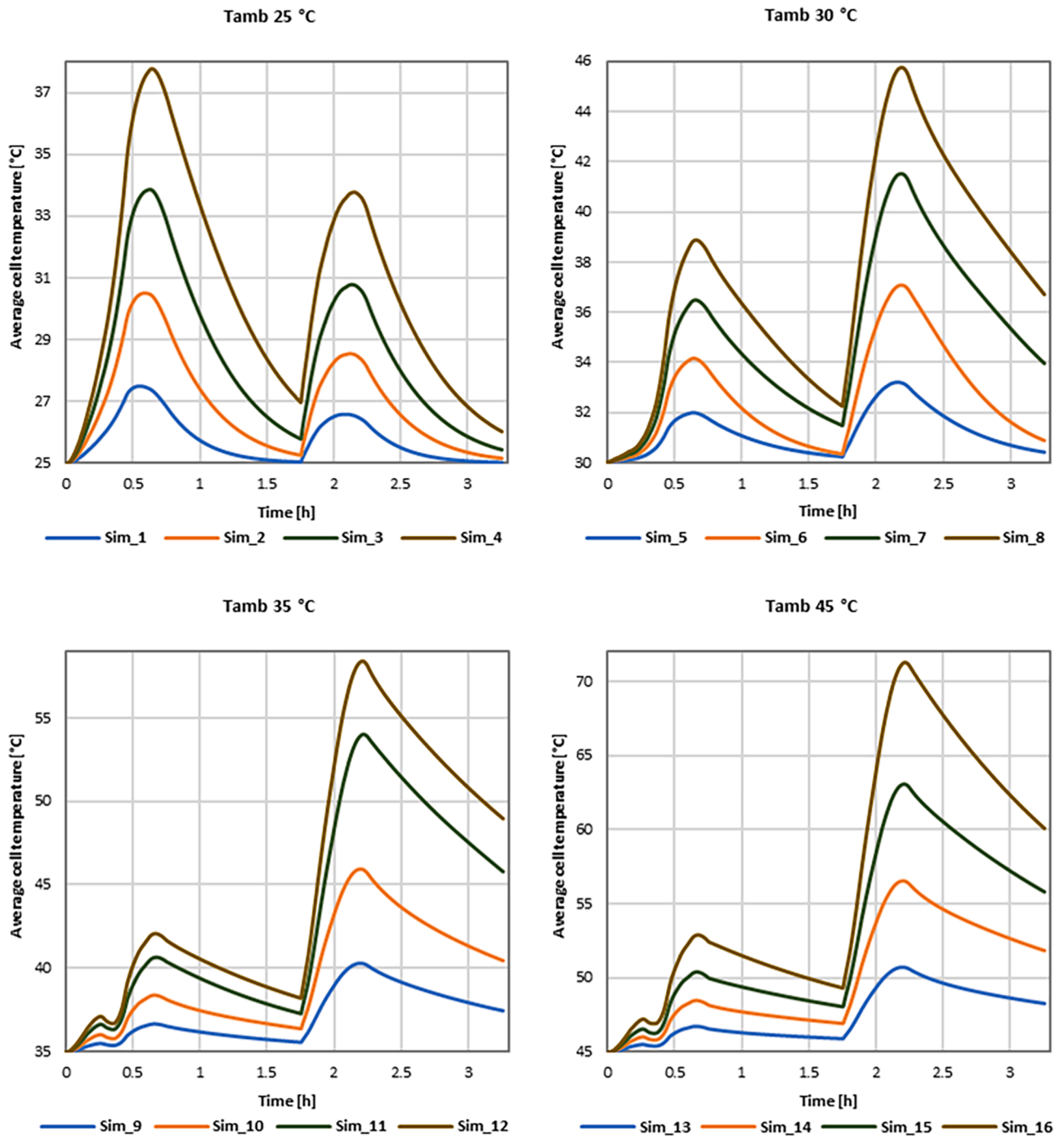
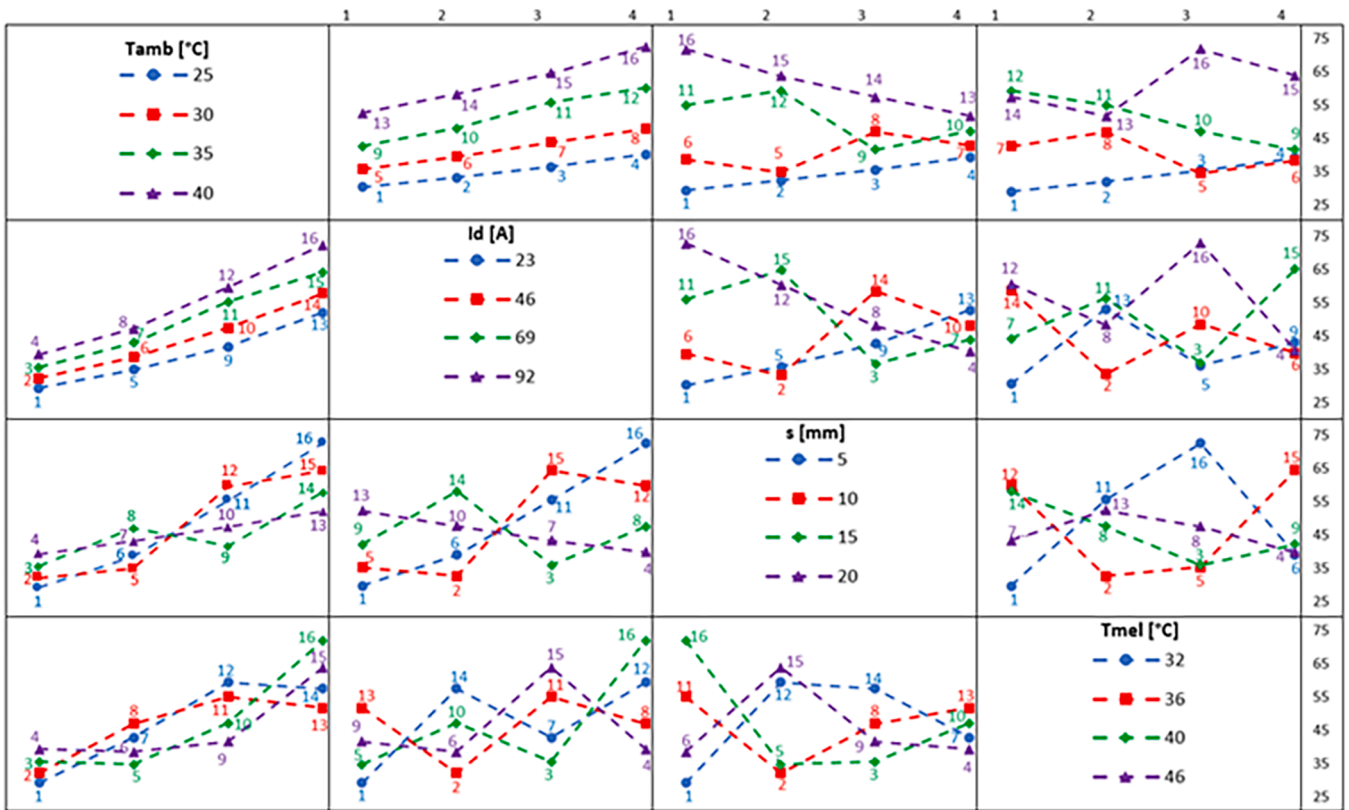**Fig. 17.** Predicted average temperature of the cell for all levels of ambient temperature.

Fig. 18. Interaction plot of the factors for each level (x-axis) on the max. cell temperature (Y-axis).
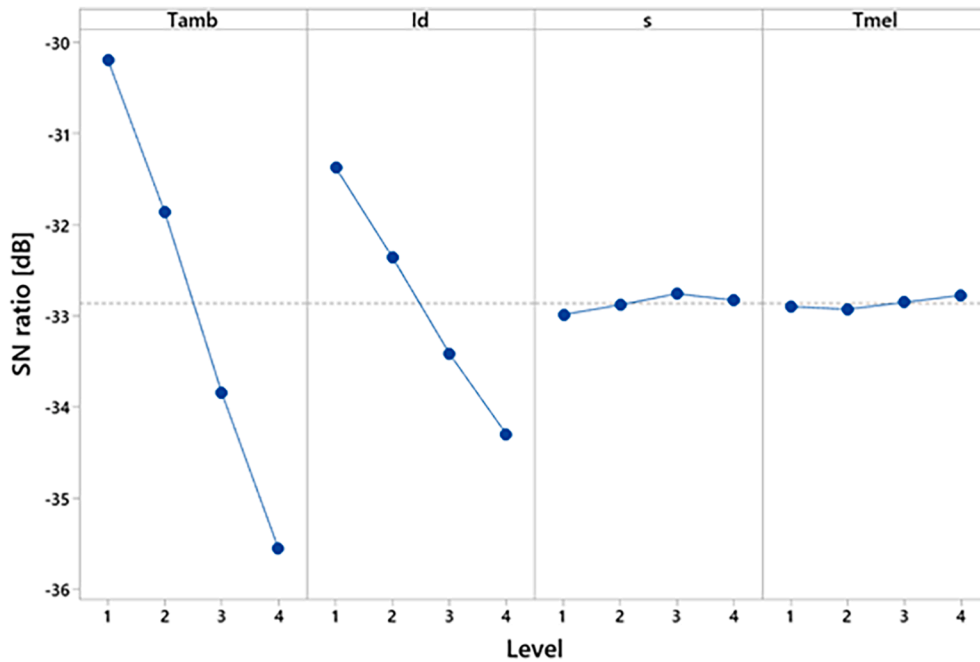

Fig. 19. S/N ratio for the four factors selected for the 16 simulations.

its values, the better the quality characteristic for the simulation. It is then defined as [80]:

$$\frac{S}{N} = -10\log\left(\frac{1}{n}\sum_{i=1}^{n}\frac{1}{y_i^2}\right) \qquad (18)$$

Where n is the number of simulations and y_i is the observation value in the i-th simulation.

The value of S/N ratio at different levels for all the factors are shown in Fig. 19. Based on the selected method for calculation (LB), it emerges that the S/N variation at various levels is more marked for the ambient

temperature and discharge current if compared to design parameters. Regarding the latter, the optimal combination is PCM thickness (L3, 15 mm) and PCM melting temperature (L3-L4, 40–46 °C). The outcome of the analysis carried out so far is that operational parameters, for the current design, are much more influential than the design ones. Accordingly, a further design enhancement is proposed and discussed in the next section.

Hybrid TMS

The results of the previous analysis indicate that further design improvement under the worst-case scenario (ambient temperature 45 °C and discharge current 92 A) requires a different TMS configuration.

The PCM-based TMS were used as starting point for the evaluation of a hybrid TMS, in which part of the heat is extracted using liquid water as coolant. As shown in Fig. 11, it mainly consists of the same passive TMS with a cooling plate on the external size with a single inlet and outlet. The size of the plate and the flow rate of the cooling water were part of

Table 10
Factors and levels selected for CFD simulations of the hybrid tms.

Levels	Factors		
	1	2	3
	u_w [m/s]	T_w [°C]	$s_{channel}$ [mm]
1	0.1	30	10
2	0.25	25	5
3	0.50	45	2.5

Table 11
Arrays selected by Taguchi's method for hybrid TMS.

Simulation	u_w [m/s]	T_w [°C]	$s_{channel}$ [mm]
1	0.1	30	10
2	0.1	25	5
3	0.1	45	2.5
4	0.25	30	5
5	0.25	25	2.5
6	0.25	45	10
7	0.5	30	2.5
8	0.5	25	10
9	0.5	45	2.5

the parametric analysis presented in the next sections. The boundary conditions (Fig. 12) used were discussed in Section 4.

For each of the factors T_w, u_w, $s_{channel}$, three levels for simulation through Taguchi's method were considered as shown in Table 10. It is worth noticing that it was also considered the worst cooling scenario corresponding to the case in which the water is at ambient temperature. The depth of the channel is a key parameter especially when seeking a space-saving design.

L9 orthogonal array

By using the Taguchi method, the number of simulations was significantly reduced, from 3^3 to 9 cases. The detailed L_9 orthogonal array generated in MATLAB software with all the simulated combinations is shown in Table 11.

The maximum temperature of the cell for the 9 simulated combination is reported in Fig. 20. According to the model results, when the temperature of the cooling water is at 45 °C, the safety conditions for Li-ion cells cannot be maintained. In detail, the maximum values exhibited by cases 3, 6, 9 were 63.26 °C, 63.34 °C, 63.28 °C, respectively. In contrast, case 5 (50.59 °C) represents the best operative condition to guarantee the thermal safety of the battery.

The big discrepancy among the various cases is due to the different temperature of the cooling water for the hybrid system. In addition to the simulated case, the result referred to the worst PCM-based system (case 16) is reported. The cooling performance η selected as indicator to assess the better thermal behaviour of the hybrid configuration was calculated as follow:

$$\eta = \frac{T_{max,PCM\_ref} - T_{max,hyb}}{T_{max,PCM\_ref}} \tag{19}$$

For the selected L_9 orthogonal array η goes from 2.34 % (case 6) to 6.04 % (case 5).

As an example of the effect of the different parameters, temporal trends including all the charge/discharge currents as for the previous tests were simulated for different temperatures of water and fluid velocity. The cases of 2.5 mm and 10 mm of channel depth are shown in Fig. 21a and Fig. 21b, respectively. It is possible to notice that, regardless of channel depth, the safety conditions cannot be maintained if the cooling water is at 45 °C (i.e. at ambient temperature). However, in order to efficiently cool down the cell and keep it within the operational
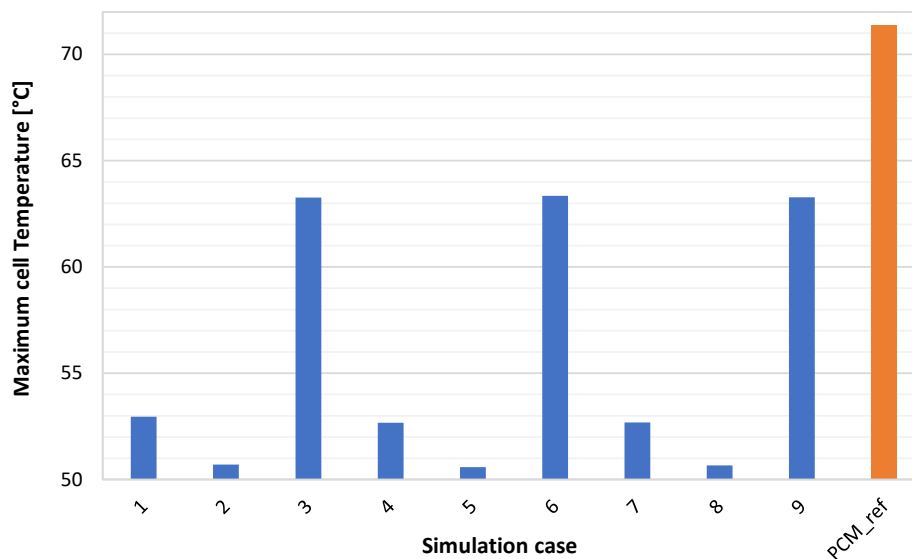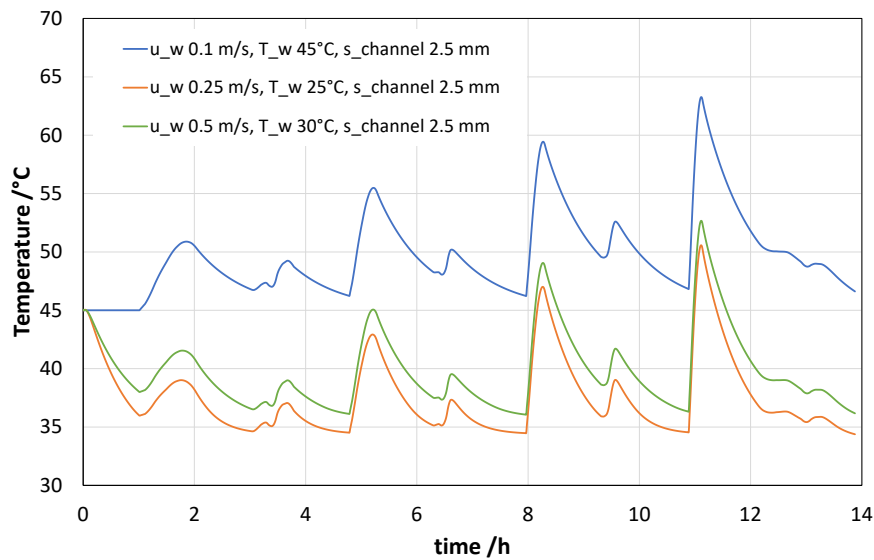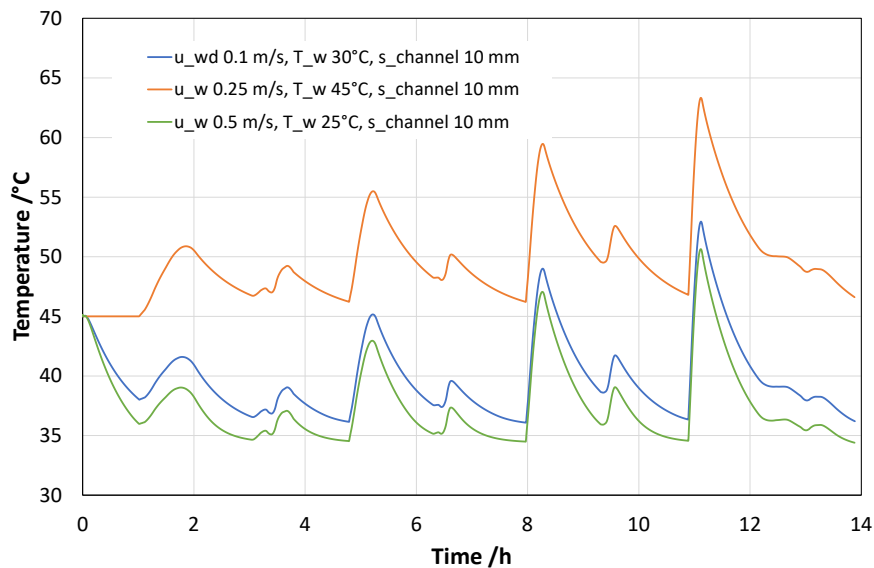

Fig. 20. Maximum cell temperature predicted for the selected 9 simulations. orange data bar refer to pcm-based tms at ambient temperature 45 °C, discharge current92 A, PCM thickness 5 mm, transition temperature 40 °C. (For interpretation of the references to colour in this figure legend, the reader is referred to the web version of this article.)

(a)

(b)

Fig. 21. Temporal trends for the hybrid tms for different temperatures and velocity of water and (a) 2.5 mm channel depth and (b) 10 mm channel depth.

range, even temperatures as high as 30 °C are allowed. Considering, for instance, the case of tap water, which is usually well below such temperatures even during summer conditions, using a fraction of tap water for cooling purposes is possible. Other possible alternatives that can allow to efficiently operate the battery without complicated or energy-expensive systems at 30 °C are evaporative coolers and solar-assisted desiccant systems [81,82].

Interaction matrix and optimal design

There is a strong dependence among the various selected factors as shown in the interaction plots depicted in Fig. 22. It is possible to notice that the curves for the different channel depths and fluid velocity are superimposed when considering variable water temperature, thus indicating that, compared to it, their influence is lower. Looking at the chart for the variable water temperature and channel depths (intersection

between the last column and the second row), it is possible to notice that a smaller channel depth is slightly better (<1°C). This result can be ascribed to the slightly higher Reynolds number and therefore a higher heat exchange between the fluid and the external surfaces. Regarding the chart for the variable fluid velocity and channel depths (intersection between the last column and the first row), it is possible to see that the higher fluid velocity leads to slightly smaller maximum temperatures. This result can again be due to a more turbulent flow into the channel. Considering for instance simulations 5 and 7, the maximum temperature increased by 2.09 °C.

The favourable value for each factor was evaluated according to the S/N ratio based on the smaller the better criterion. The value of S/N ratio for the selected L_9 orthogonal array is shown in Fig. 23. It is possible to notice that the influence of the fluid velocity and channel depth is negligible. Indeed, for the conditions selected, Reynolds number
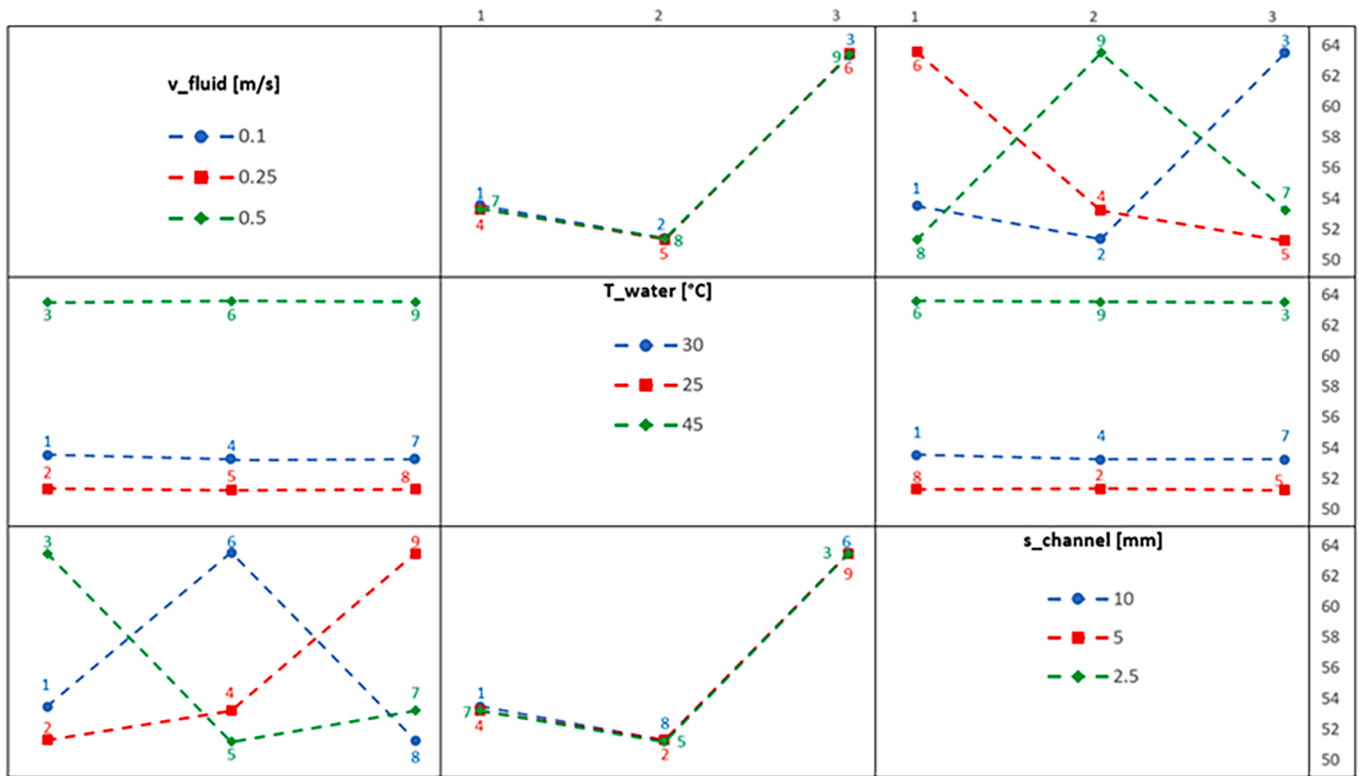
Fig. 22. Interaction plot for the three factors selected in the hybrid tms.
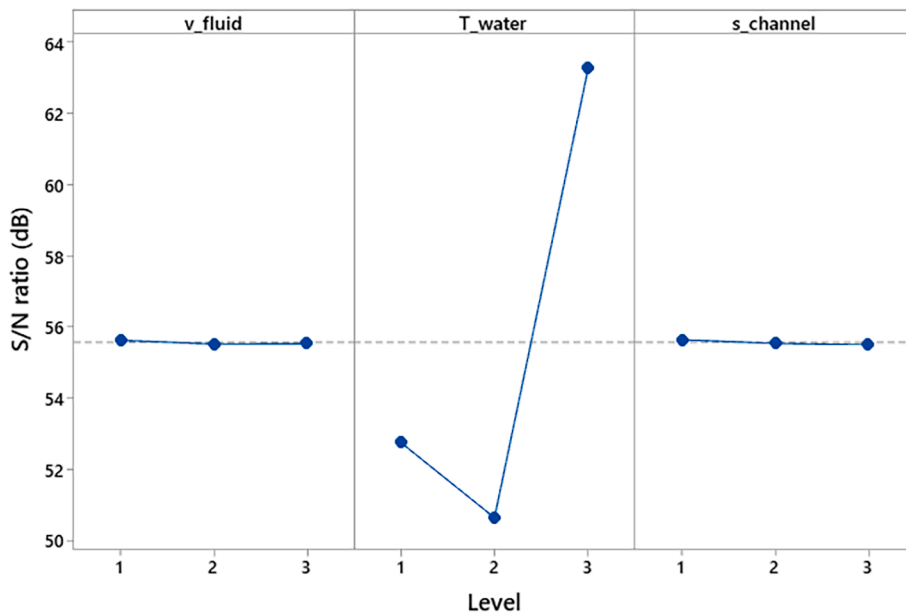

Fig. 23. S/N ratio for the three factors selected for the 9 simulations.

in the liquid channel ranges from 6300 to 12000, meaning the flow is always turbulent and is enough to guarantee good heat transfer. Considering that channel depth is not a critical parameter, compared to the temperature of the water, this means that a space-saving design is possible by selecting the smaller value (2.5 mm) among the considered ones.

A comparison among the different battery designs is reported in Fig. 24. The same discharge current (92 A) and ambient temperature (45 °C) are considered. Regarding the PCM, thickness of 10 mm and melting temperature of 40 °C were chosen. For the hybrid system, additional parameters for the case shown in the comparison are speed of the fluid of 0.5 m/s, channel depth of 2.5 mm and cooling water temperature of 30 °C. It is possible to notice that, under the extreme conditions considered, i.e. high-current applications and very warm ambient temperatures, only the hybrid TMS guarantees safe operation. In the case of the hybrid TMS, if compared to the natural cooling, the reduction in maximum cell temperature is 22 K, whereas for the passive TMS is 11 K.
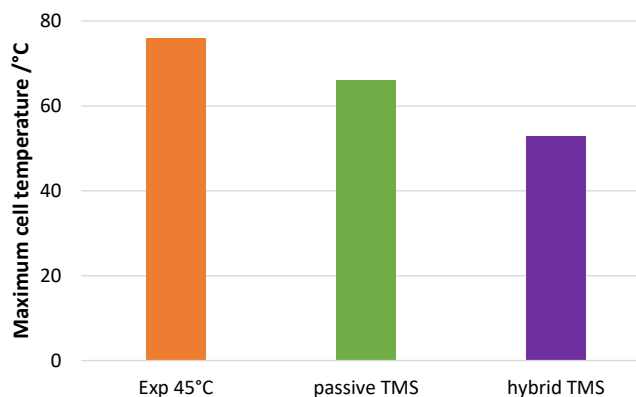
Fig. 24. Comparison of maximum cell temperature for the case of natural cooling, passive tms and hybrid tms.

Conclusions

The paper discusses a systematic methodology for the design of a thermal management system for a Li-ion battery cell working under different operating conditions. The cell was characterized experimentally via thermal and electric tests carried out at different ambient temperatures and in charge/discharge cycles at different C-rates. The results clearly indicated that, unless a thermal management system is foreseen, it is not recommended to operate the cell under high current and high ambient temperature. A numerical model was implemented in the software COMSOL Multiphysics® 5.6, and was validated with experimental results, showing a reliable prediction of the external surface temperature of the cell. Then the model was used to perform a parametric analysis of a PCM-based passive system aiming at investigating the effect of operating conditions (ambient temperature and discharge current) and design features (PCM layer thickness and phase change temperature). The minimum number of simulations required to analyse the effect of the parameters was identified through Taguchi's method. Model predictions showed that the PCM improved the temperature uniformity and held the maximum temperature of the cell. In the worst case (ambient temperature of 45 °C and discharge current 92 A) 5 mm thick PCM layer with transition temperature of 40 °C reduced the maximum temperature by 4.61 °C. Ambient temperature below 45 °C, discharge current below 92 A, PCM layer thickness above 10 mm and transition temperature above 40 °C were identified as recommended values to guarantee the thermal safety of the battery. The combined effects of the operating conditions and design parameters were discussed through interaction plots and S/N analysis. It was shown that ambient temperature and discharge current have a high effect on the maximum temperature reached during operation, whereas the performance of the thermal management systems were less affected by the change in the design parameters (transition temperature and PCM layer thickness). With the passive system at higher temperatures and for subsequent charge/discharge cycles at high current the battery not always worked within the optimal range of safe temperature (<60 °C). For this reason, the best conditions identified in terms of PCM thickness and melting temperature (10 mm and 40 °C, respectively) were then used for the design of a hybrid thermal management system consisting of a jacket with water as coolant around the PCM layer. Parametric simulations, selected again with the orthogonal array method, were carried out to evaluate the effect of fluid velocity, coolant temperature and channel depth. A water temperature of 25 °C and a channel of 2.5 mm thick led to an increase in the cooling performance by 6.04 % under extreme ambient temperature and discharge current conditions (45 °C and 92 A). Interaction plots and S/N analysis shown that the cooling water is the most influential parameter. PCM melting temperature of 40 °C, PCM thickness of 10 mm, channel depth of 2.5 mm, cooling water inlet temperature of 30 °C were identified as the optimal parameters for the

hybrid TMS. In detail, the reduction in the in maximum cell temperature was 22 °C and 11 °C compared to the naturally air cooled cell and PCM-based thermal management system, respectively.

The results here presented indicate that the proposed methodology allows a computationally cheap and yet effective design of a thermal management system for batteries even under off-design conditions.

The proposed methodology can be used to conduct future studies extending the optimization analysis to further configurations including (i) different PCM materials, (ii) different coolant fluids, (III) multicell battery arrays in high power applications. Accordingly, it can be concluded that the main outcome from the paper is a highly reusable methodology, that can be replicated for the evaluation of different types of TMS, with different coolant, PCM materials and operating conditions (charge/discharge rates). Further activities will be carried out for the experimental validation of the hybrid system and its practical application in pilots' activities.

CRediT authorship contribution statement

Girolama Airò Farulla: Visualization, Formal analysis, Investigation, Conceptualization, Writing – original draft. **Valeria Palomba:** Data curation, Formal analysis, Investigation, Methodology, Validation, Conceptualization, Writing – original draft. **Davide Aloisio:** Data curation, Visualization, Formal analysis, Investigation, Methodology, Validation, Conceptualization, Writing – original draft. **Giovanni Brunaccini:** Data curation, Visualization, Methodology, Writing – original draft, Writing – review & editing. **Marco Ferraro:** Project administration, Supervision, Resources, Writing – original draft, Writing – review & editing. **Andrea Frazzica:** Project administration, Supervision, Visualization, Resources, Methodology, Writing – original draft, Writing – review & editing. **Francesco Sergi:** Funding acquisition, Resources, Project administration, Supervision, Writing – original draft, Writing – review & editing.

Declaration of Competing Interest

The authors declare that they have no known competing financial interests or personal relationships that could have appeared to influence the work reported in this paper.

Data availability

Data will be made available on request.

Acknowledgements

Reference

[1] S. Koohi-Fayegh, M.A. Rosen, A review of energy storage types, applications and recent developments, J. Energy Storage 27 (2020), 101047, https://doi.org/10.1016/j.est.2019.101047.

[2] S.G. Leonardi, D. Aloisio, G. Brunaccini, A. Stassi, M. Ferraro, V. Antonucci, F. Sergi, Investigation on the ageing mechanism for a lithium-ion cell under accelerated tests: the case of primary frequency regulation service, J. Energy Storage 41 (2021), 102904, https://doi.org/10.1016/j.est.2021.102904.

[3] S. Micari, S. Foti, A. Testa, S. De Caro, F. Sergi, L. Andaloro, D. Aloisio, G. Napoli, Reliability assessment and lifetime prediction of Li-ion batteries for electric vehicles, Electr. Eng. 104 (2022) 165–177, https://doi.org/10.1007/s00202-021-01288-4.

[4] P. Sun, X. Zhang, S. Wang, Y. Zhu, Lithium-ion battery degradation caused by overcharging at low temperatures, Therm. Sci. Eng. Prog. 30 (2022), 101266, https://doi.org/10.1016/j.tsep.2022.101266.

[5] S. Arora, A. Kapoor, W. Shen, A novel thermal management system for improving discharge/charge performance of Li-ion battery packs under abuse, J. Power Sources 378 (2018) 759–775, https://doi.org/10.1016/j.jpowsour.2017.12.030.

[6] V.G. Choudhari, D.A.S. Dhoble, T.M. Sathe, A review on effect of heat generation and various thermal management systems for lithium ion battery used for electric vehicle, J. Energy Storage 32 (2020), 101729, https://doi.org/10.1016/j.est.2020.101729.

[7] J. Gou, W. Liu, Y. Luo, The thermal performance of a novel internal cooling method for the electric vehicle battery: an experimental study, Appl. Therm. Eng. 161 (2019), 114102, https://doi.org/10.1016/j.applthermaleng.2019.114102.

[8] Y. Zeng, D. Chalise, S.D. Lubner, S. Kaur, R.S. Prasher, A review of thermal physics and management inside lithium-ion batteries for high energy density and fast charging, Energy Storage Mater. 41 (2021) 264–288, https://doi.org/10.1016/j.ensm.2021.06.008.

[9] C.H. Doh, Y.C. Ha, S. Wook Eom, Entropy measurement of a large format lithium ion battery and its application to calculate heat generation, Electrochim. Acta 309 (2019) 382–391, https://doi.org/10.1016/J.ELECTACTA.2019.04.026.

[10] J. Weng, Q. Huang, X. Li, G. Zhang, D. Ouyang, M. Chen, A.C.Y. Yuen, A. Li, E.W. M. Lee, W. Yang, J. Wang, X. Yang, Safety issue on PCM-based battery thermal management: material thermal stability and system hazard mitigation, Energy Storage Mater. 53 (2022) 580–612, https://doi.org/10.1016/j.ensm.2022.09.007.

[11] P. Lyu, X. Liu, J. Qu, J. Zhao, Y. Huo, Z. Qu, Z. Rao, Recent advances of thermal safety of lithium ion battery for energy storage, Energy Storage Mater. 31 (2020) 195–220, https://doi.org/10.1016/j.ensm.2020.06.042.

[12] S. Yang, Y. Hua, D. Qiao, Y. Lian, Y. Pan, Y. He, A coupled electrochemical-thermal-mechanical degradation modelling approach for lifetime assessment of lithium-ion batteries, Electrochim. Acta 326 (2019), 134928, https://doi.org/10.1016/j.electacta.2019.134928.

[13] Y. Yang, L. Chen, K. Tong, L. Yang, K. Jiang, Y. Kong, X. Du, Thermal-electrical characteristics of lithium-ion battery module in series connection with a hybrid cooling, Int. J. Heat Mass Transf. 184 (2022), 122309, https://doi.org/10.1016/j.ijheatmasstransfer.2021.122309.

[14] T. He, T. Zhang, Z. Wang, Q. Cai, A comprehensive numerical study on electrochemical-thermal models of a cylindrical lithium-ion battery during discharge process, Appl. Energy 313 (2022), 118797, https://doi.org/10.1016/j.apenergy.2022.118797.

[15] H. Behi, D. Karimi, J. Jaguemont, F.H. Gandoman, T. Kalogiannis, M. Berecibar, J. Van Mierlo, Novel thermal management methods to improve the performance of the Li-ion batteries in high discharge current applications, Energy 224 (2021), 120165, https://doi.org/10.1016/j.energy.2021.120165.

[16] A. Maheshwari, M.A. Dumitrescu, M. Destro, M. Santarelli, A MODELLING APPROACH TO UNDERSTAND CHARGE DISCHARGE DIFFERENCES IN THERMAL BEHAVIOUR IN LITHIUM IRON PHOSPHATE – GRAPHITE BATTERY, Electrochim. Acta 243 (2017) 129–141, https://doi.org/10.1016/j.electacta.2017.05.049.

[17] H. Ruan, J. Jiang, B. Sun, W. Gao, L. Wang, W. Zhang, Online estimation of thermal parameters based on a reduced wide-temperature-range electro-thermal coupled model for lithium-ion batteries, J. Power Sources 396 (2018) 715–724, https://doi.org/10.1016/j.jpowsour.2018.03.075.

[18] J. He, M. Sazzad Hosen, R. Youssef, T. Kalogiannis, J. Van Mierlo, M. Berecibar, A lumped electro-thermal model for a battery module with a novel hybrid cooling system, Appl. Therm. Eng. 221 (2023), 119874, https://doi.org/10.1016/J.APPLTHERMALENG.2022.119874.

[19] P. Jindal, P. Sharma, M. Kundu, S. Singh, D.K. Shukla, V.J. Pawar, Y. Wei, P. Breedon, Computational Fluid Dynamics (CFD) analysis of Graphene Nanoplatelets for the cooling of a multiple tier Li-ion battery pack, Therm. Sci. Eng. Prog. 31 (2022) 101282.

[20] Y. Shi, S. Ahmad, H. Liu, K.T. Lau, J. Zhao, Optimization of air-cooling technology for LiFePO$_4$ battery pack based on deep learning, J. Power Sources 497 (2021), 229894, https://doi.org/10.1016/J.JPOWSOUR.2021.229894.

[21] B. Wu, S. Han, K.G. Shin, W. Lu, Application of artificial neural networks in design of lithium-ion batteries, J. Power Sources 395 (2018) 128–136, https://doi.org/10.1016/J.JPOWSOUR.2018.05.040.

[22] X. Qian, D. Xuan, X. Zhao, Z. Shi, Heat dissipation optimization of lithium-ion battery pack based on neural networks, Appl. Therm. Eng. 162 (2019), 114289, https://doi.org/10.1016/J.APPLTHERMALENG.2019.114289.

[23] F. Feng, S. Teng, K. Liu, J. Xie, Y. Xie, B. Liu, K. Li, Co-estimation of lithium-ion battery state of charge and state of temperature based on a hybrid electrochemical-thermal-neural-network model, J. Power Sources. 455 (2020), 227935, https://doi.org/10.1016/J.JPOWSOUR.2020.227935.

[24] W. Wu, Q.N. Chan, S. Kook, G.H. Yeoh, Integration of Computational Fluid Dynamics and Artificial Neural Network for Optimization Design of Battery Thermal Management System, (2022).

[25] Y.W. Wang, C.M. Shu, Energy generation mechanisms for a Li-ion cell in case of thermal explosion: a review, J. Energy Storage 55 (2022), 105501, https://doi.org/10.1016/j.est.2022.105501.

[26] G. Xu, L. Huang, C. Lu, X. Zhou, G. Cui, Revealing the multilevel thermal safety of lithium batteries, Energy Storage Mater. 31 (2020) 72–86, https://doi.org/10.1016/j.ensm.2020.06.004.

[27] C. Wang, C. Li, G. Wang, C. Zhang, N. Cui, Fast identification method for thermal model parameters of Lithium-ion battery based on discharge temperature rise, J. Energy Storage 44 (2021), 103362, https://doi.org/10.1016/j.est.2021.103362.

[28] A. Mevawalla, S. Panchal, M.-K. Tran, M. Fowler, R. Fraser, Mathematical heat transfer modeling and experimental validation of lithium-ion battery considering: tab and surface temperature, separator, electrolyte resistance, anode-cathode irreversible and reversible heat, Batteries 6 (2020) 61, https://doi.org/10.3390/batteries6040061.

[29] M.W. Nazar, N. Iqbal, M. Ali, H. Nazir, M.Z. Bin Amjad, Thermal management of Li-ion battery by using active and passive cooling method, J. Energy Storage. 61 (2023), 106800, https://doi.org/10.1016/j.est.2023.106800.

[30] X. Zhang, Z. Li, L. Luo, Y. Fan, Z. Du, A review on thermal management of lithium-ion batteries for electric vehicles, Energy. 238 (2022), 121652, https://doi.org/10.1016/j.energy.2021.121652.

[31] O. Teichert, F. Müller, M. Lienkamp, Techno-economic design of battery thermal management systems in different climates, J. Energy Storage. 48 (2022), 103832, https://doi.org/10.1016/j.est.2021.103832.

[32] J. Luo, D. Zou, Y. Wang, S. Wang, L. Huang, Battery thermal management systems (BTMs) based on phase change material (PCM): a comprehensive review, Chem. Eng. J. 430 (2022), 132741, https://doi.org/10.1016/j.cej.2021.132741.

[33] H. Fayaz, A. Afzal, A.D.M. Samee, M.E.M. Soudagar, N. Akram, M.A. Mujtaba, R.D. Jilte, M.T. Islam, Ü. Ağbulut, C.A. Saleel, Optimization of Thermal and Structural Design in Lithium-Ion Batteries to Obtain Energy Efficient Battery Thermal Management System (BTMS): A Critical Review, Springer Netherlands, 2022. https://doi.org/10.1007/s11831-021-09571-0.

[34] B. Lamrani, B.E. Lebrouhi, Y. Khattari, T. Kousksou, A simplified thermal model for a lithium-ion battery pack with phase change material thermal management system, J. Energy Storage 44 (2021), 103377, https://doi.org/10.1016/j.est.2021.103377.

[35] M.M. Heyhat, S. Mousavi, M. Siavashi, Battery thermal management with thermal energy storage composites of PCM, metal foam, fin and nanoparticle, J. Energy Storage 28 (2020), 101235, https://doi.org/10.1016/j.est.2020.101235.

[36] A. Hussain, C.Y. Tso, C.Y.H. Chao, Experimental investigation of a passive thermal management system for high-powered lithium ion batteries using nickel foam-paraffin composite, Energy 115 (2016) 209–218, https://doi.org/10.1016/j.energy.2016.09.008.

[37] M.M. El Idi, M. Karkri, M. Abdou Tankari, A passive thermal management system of Li-ion batteries using PCM composites: experimental and numerical investigations, Int. J. Heat Mass Transf. 169 (2021), 120894, https://doi.org/10.1016/j.ijheatmasstransfer.2020.120894.

[38] B. Buonomo, D. Ercole, O. Manca, F. Menale, Thermal cooling behaviors of lithium-ion batteries by metal foam with phase change materials, Energy Procedia 148 (2018) 1175–1182, https://doi.org/10.1016/j.egypro.2018.08.024.

[39] Z. Wang, H. Zhang, X. Xia, Experimental investigation on the thermal behavior of cylindrical battery with composite paraffin and fin structure, Int. J. Heat Mass Transf. 109 (2017) 958–970, https://doi.org/10.1016/j.ijheatmasstransfer.2017.02.057.

[40] Z. Sun, R. Fan, F. Yan, T. Zhou, N. Zheng, Thermal management of the lithium-ion battery by the composite PCM-Fin structures, Int. J. Heat Mass Transf. 145 (2019), 118739, https://doi.org/10.1016/j.ijheatmasstransfer.2019.118739.

[41] J. Weng, Y. He, D. Ouyang, X. Yang, G. Zhang, J. Wang, Thermal performance of PCM and branch-structured fins for cylindrical power battery in a high-temperature environment, Energy Convers. Manag. 200 (2019), 112106, https://doi.org/10.1016/j.enconman.2019.112106.

[42] J. Zhang, D. Shao, L. Jiang, G. Zhang, H. Wu, R. Day, W. Jiang, Advanced thermal management system driven by phase change materials for power lithium-ion batteries: a review, Renew. Sustain. Energy Rev. 159 (2022) 112207, https://doi.org/10.1016/j.rser.2022.112207.

[43] Y. Zhang, J. Huang, M. Cao, Z. Liu, Q. Chen, A novel flexible phase change material with well thermal and mechanical properties for lithium batteries application, J. Energy Storage 44 (2021), 103433, https://doi.org/10.1016/j.est.2021.103433.

[44] A. Verma, S. Shashidhara, D. Rakshit, A comparative study on battery thermal management using phase change material (PCM), Therm. Sci. Eng. Prog. 11 (2019) 74–83, https://doi.org/10.1016/j.tsep.2019.03.003.

[45] R. Zhao, J. Gu, J. Liu, Optimization of a phase change material based internal cooling system for cylindrical Li-ion battery pack and a hybrid cooling design, Energy 135 (2017) 811–822, https://doi.org/10.1016/j.energy.2017.06.168.

[46] H. Yang, H. Li, Z. Wang, B. Ma, A compact and lightweight hybrid liquid cooling system coupling with Z-type cold plates and PCM composite for battery thermal management, Energy 263 (2023), 126026, https://doi.org/10.1016/j.energy.2022.126026.

[47] A.G. Mohammed, K.E. Elfeky, Q. Wang, Recent advancement and enhanced battery performance using phase change materials based hybrid battery thermal management for electric vehicles, Renew. Sustain. Energy Rev. 154 (2022), 111759, https://doi.org/10.1016/j.rser.2021.111759.

[48] G. Zhao, X. Wang, M. Negnevitsky, C. Li, An up-to-date review on the design improvement and optimization of the liquid-cooling battery thermal management system for electric vehicles, Appl. Therm. Eng. 219 (2023), 119626, https://doi.org/10.1016/j.applthermaleng.2022.119626.

[49] P. Zare, N. Perera, J. Lahr, R. Hasan, Solid-liquid phase change materials for the battery thermal management systems in electric vehicles and hybrid electric vehicles – A systematic review, J. Energy Storage 52 (2022) 105026, https://doi.org/10.1016/j.est.2022.105026.

[50] A. Angani, H.-W. Kim, M.-H. Hwang, E. Kim, K.-M. Kim, H.-R. Cha, A comparison between Zig-Zag plated hybrid parallel pipe and liquid cooling battery thermal management systems for Lithium-ion battery module, Appl. Therm. Eng. 219 (2023), 119599, https://doi.org/10.1016/j.applthermaleng.2022.119599.

[51] W. Zeng, Y. Niu, S. Li, S. Hu, B. Mao, Y. Zhang, Cooling performance and optimization of a new hybrid thermal management system of cylindrical battery, Appl. Therm. Eng. 217 (2022), 119171, https://doi.org/10.1016/j.applthermaleng.2022.119171.

[52] X. Liu, C.-F. Zhang, J.-G. Zhou, X. Xiong, C.-C. Zhang, Y.-P. Wang, Numerical simulation of hybrid battery thermal management system combining thermoelectric cooler and phase change material, Energy Rep. 8 (2022) 1094–1102, https://doi.org/10.1016/j.egyr.2022.11.003.

[53] M. Faizan, S. Pati, P. Randive, Implications of novel cold plate design with hybrid cooling on thermal management of fast discharging lithium-ion battery, J. Energy Storage 53 (2022), 105051, https://doi.org/10.1016/j.est.2022.105051.

[54] Y. Zhao, B. Zou, J. Ding, Y. Ding, Experimental and numerical investigation of a hybrid battery thermal management system based on copper foam-paraffin composite phase change material and liquid cooling, Appl. Therm. Eng. 218 (2023), 119312, https://doi.org/10.1016/j.applthermaleng.2022.119312.

[55] Y. Zhuang, T. Chen, J. Chen, J. Li, M. Guan, Y. Chen, Thermal uniformity performance of a hybrid battery thermal management system using phase change material and cooling plates arrayed in the manner of honeycomb, Therm. Sci. Eng. Prog. 26 (2021) 101094, https://doi.org/10.1016/j.tsep.2021.101094.

[56] Y. Wang, T. Gao, L. Zhou, J. Gong, J. Li, A parametric study of a hybrid battery thermal management system that couples PCM with wavy microchannel cold plate, Appl. Therm. Eng. 219 (2023), 119625, https://doi.org/10.1016/j.applthermaleng.2022.119625.

[57] X. Wu, K. Wang, Z. Chang, Y. Chen, S. Cao, C. Lv, H. Liu, Y. Wang, Experimental and numerical study on hybrid battery thermal management system combining liquid cooling with phase change materials, Int. Commun. Heat Mass Transf. 139 (2022), 106480, https://doi.org/10.1016/j.icheatmasstransfer.2022.106480.

[58] K.A.M. Alharbi, G.F. Smaisim, S.M. Sajadi, M.A. Fagiry, H.Ş. Aybar, S.E. Elkhatib, Numerical study of lozenge, triangular and rectangular arrangements of lithium-ion batteries in their thermal management in a cooled-air cooling system, J. Energy Storage 52 (2022), 104786, https://doi.org/10.1016/j.est.2022.104786.

[59] H. Behi, D. Karimi, T. Kalogiannis, J. He, M.S. Patil, J.-D. Muller, A. Haider, J. Van Mierlo, M. Berecibar, Advanced hybrid thermal management system for LTO battery module under fast charging, Case Stud. Therm. Eng. 33 (2022), 101938, https://doi.org/10.1016/j.csite.2022.101938.

[60] S.A. Khan, C. Eze, K. Dong, A.R. Shahid, M.S. Patil, S. Ahmad, I. Hussain, J. Zhao, Design of a new optimized U-shaped lightweight liquid-cooled battery thermal management system for electric vehicles: a machine learning approach, Int. Commun. Heat Mass Transf. 136 (2022), 106209, https://doi.org/10.1016/j.icheatmasstransfer.2022.106209.

[61] A. Shahsavar, A. Goodarzi, I. Baniasad Askari, M. Jamei, M. Karbasi, M. Afrand, The entropy generation analysis of the influence of using fins with tip clearance on the thermal management of the batteries with phase change material: application a new gradient-based ensemble machine learning approach, Eng. Anal. Bound. Elem. 140 (2022) 432–446, https://doi.org/10.1016/j.enganabound.2022.04.024.

[62] S. Aggarwal, S. Thareja, A. Verma, T.R. Bhardwaj, M. Kumar, An overview on 5α-reductase inhibitors, Steroids 75 (2010) 109–153, https://doi.org/10.1016/j.steroids.2009.10.005.

[63] F. Sergi, G. Brunaccini, D. Aloisio, N. Randazzo, R.M. Polito, M. Pietrucci, M. G. Fadda, M. Ferraro, V. Antonucci, Evaluation of a Li-Titanate battery module in primary frequency control ancillary service conditions, J. Energy Storage. 24 (2019), 100805, https://doi.org/10.1016/j.est.2019.100805.

[64] S. Thanagasundram, R. Arunachala, K. Makinejad, T. Teutsch, A. Jossen, EEVC European Electric Vehicle Congress A Cell Level Model for Battery Simulation, (n. d.).

[65] H. Zuo, B. Zhang, Z. Huang, K. Wei, H. Zhu, J. Tan, Effect analysis on SOC values of the power lithium manganate battery during discharging process and its intelligent estimation, Energy 238 (2022), 121854, https://doi.org/10.1016/j.energy.2021.121854.

[66] H. Pang, L.-J. Mou, L. Guo, Parameter identification and state-of-charge estimation approach for enhanced lithium–ion battery equivalent circuit model considering influence of ambient temperatures*, Chinese Phys. B. 28 (10) (2019) 108201.

[67] F. Sergi, A. Arista, G. Agnello, M. Ferraro, L. Andaloro, V. Antonucci, Characterization and comparison between lithium iron phosphate and lithium-polymers batteries, J. Energy Storage 8 (2016) 235–243, https://doi.org/10.1016/j.est.2016.08.012.

[68] M.J. Lain, E. Kendrick, Understanding the limitations of lithium ion batteries at high rates, J. Power Sources 493 (2021), 229690, https://doi.org/10.1016/j.jpowsour.2021.229690.

[69] I. Baccouche, S. Jemmali, A. Mlayah, B. Manai, N.E. Ben Amara, Implementation of an improved coulomb-counting algorithm based on a piecewise SOC-OCV relationship for SOC estimation of Li-Ion battery, Int. J. Renew. Energy Res. 8 (2018) 178–187. https://doi.org/10.20508/ijrer.v8i1.6686.g7292.

[70] X. Han, M. Ouyang, L. Lu, J. Li, Cycle life of commercial lithium-ion batteries with lithium titanium oxide anodes in electric vehicles, Energies. 7 (2014) 4895–4909, https://doi.org/10.3390/en7084895.

[71] W. Mei, H. Li, C. Zhao, J. Sun, Q. Wang, Numerical study on thermal characteristics comparison between charge and discharge process for lithium ion battery, Int. J. Heat Mass Transf. 162 (2020), 120319, https://doi.org/10.1016/j.ijheatmasstransfer.2020.120319.

[72] P.-J. Alphonse, G. Elden, THE INVESTIGATION OF THERMAL BEHAVIOR IN A VANADIUM REDOX FLOW BATTERY DURING CHARGE AND DISCHARGE PROCESSES, J. Energy Storage 40 (2021), 102770, https://doi.org/10.1016/j.est.2021.102770.

[73] P. Jindal, R. Katiyar, J. Bhattacharya, Evaluation of accuracy for Bernardi equation in estimating heat generation rate for continuous and pulse-discharge protocols in LFP and NMC based Li-ion batteries, Appl. Therm. Eng. 201 (2022), 117794, https://doi.org/10.1016/j.applthermaleng.2021.117794.

[74] F.P. Incropera, D.P. DeWitt, T.L. Bergman, A.S. Lavine, Heat and mass transfer - Incropera 6e, Fundam. Heat Mass Transf. (2007).

[75] G. Zhang, N. Xiao, B. Wang, A.G. Razaqpur, Thermal performance of a novel building wall incorporating a dynamic phase change material layer for efficient utilization of passive solar energy, Constr. Build. Mater. 317 (2022), 126017, https://doi.org/10.1016/j.conbuildmat.2021.126017.

[76] Y.-W. Leung, Y. Wang, An orthogonal genetic algorithm with quantization for global numerical optimization, IEEE Trans. Evol. Comput. 5 (2001) 41–53, https://doi.org/10.1109/4235.910464.

[77] S. Ma, M. Jiang, P. Tao, C. Song, J. Wu, J. Wang, T. Deng, W. Shang, Temperature effect and thermal impact in lithium-ion batteries: a review, Prog. Nat. Sci. Mater. Int. 28 (6) (2018) 653–666.

[78] Y. Du, S. Shironita, E. Hosono, D. Asakura, Y. Sone, M. Umeda, Differences in the deterioration behaviors of fast-charged lithium-ion batteries at high and low temperatures, J. Power Sources 556 (2023), 232513, https://doi.org/10.1016/j.jpowsour.2022.232513.

[79] W. Lin, Z. Ma, H. Ren, S. Gschwander, S. Wang, Multi-objective optimisation of thermal energy storage using phase change materials for solar air systems, Renew. Energy 130 (2019) 1116–1129, https://doi.org/10.1016/j.renene.2018.08.071.

[80] S. Ata, A. Kahraman, R. Şahin, Prediction and sensitivity analysis under different performance indices of R1234ze ORC with Taguchi's multi-objective optimization, Case Stud. Therm. Eng. 22 (2020), 100785, https://doi.org/10.1016/j.csite.2020.100785.

[81] A. Tejero-González, M. Andrés-Chicote, P. García-Ibáñez, E. Velasco-Gómez, F. J. Rey-Martínez, Assessing the applicability of passive cooling and heating techniques through climate factors: an overview, Renew. Sustain. Energy Rev. 65 (2016) 727–742, https://doi.org/10.1016/j.rser.2016.06.077.

[82] A. Frein, M. Muscherà, R. Scoccia, M. Aprile, M. Motta, Field testing of a novel hybrid solar assisted desiccant evaporative cooling system coupled with a vapour compression heat pump, Appl. Therm. Eng. 130 (2018) 830–846, https://doi.org/10.1016/j.applthermaleng.2017.10.168.